
Overview: “Children’s Toxicology”, a renovating study field of irreversible “early exposure-delayed effects”

Jun Kanno

Division of Cellular and Molecular Toxicology, Biological Safety Research Center, National Institute of Health Sciences, 1-18-1 Kamiyoga, Setagaya-ku, Tokyo 158-8501, Japan

(Received February 17, 2009)

ABSTRACT — “Children are not small adults”. This is a well-known phrase, especially in the clinics for diagnosis, efficacy of treatment, side effect, and prognosis. However, in the field of toxicology, this issue has long been a challenge. The knowledge has been limited to the differences in metabolism and other physiological factors. Currently available test guidelines for fetuses and immature animals are teratogenicity and reproductive toxicity studies. These tests look for straight-forward (essentially macroscopic) outcomes established within a rather short period of exposure to the test substances. However, recent advances in molecular toxicology allow combination of *in vitro* and *in vivo* studies at molecular levels. The target molecules and receptors can be identified in quantitative fashion and at the fine structure levels around and below the resolution of normal light microscopy. Such expansion of the knowledge lead us to consider a rather new category of “receptor mediated toxicity” or “signal toxicity”. Such non-organic insults would merely induce transient effects on adults. However, there are growing evidences that such slight insults on the developing and maturing organisms can leave irreversible effects that become overt in adulthood. As an overview, toxicology has entered a new phase where children’s toxicology becomes a renovating study field of the irreversible “early exposure-delayed effects”.

Key words: Children’s toxicology, Receptor-mediated toxicity, Signal toxicity, Early exposure-delayed effect

INTRODUCTION

Toxicology is a study to analyze interaction between living organisms and xenobiotics, and its final goal is to secure the safety of humans and environment in modern life where various products and technologies are used. Up to now, the majority of toxicological tests to evaluate the toxicity of a particular substance are utilizing experimental animals as a surrogate of humans. The results obtained from such animal tests are extrapolated to humans for the settlement of various kinds of regulation on the test substances, i.e. food additives, pesticides, industrial chemicals, medicines, etc. In cases of pharmaceutical products, clinical trials (human tests) are available. However, these are rather exceptional occasions for toxicology as a whole. It would be very difficult for non-pharmaceutical objects to test on humans, and even for pharmaceuticals, human trial for children including fetuses have many difficulties.

Current toxicological testing protocols are based on an assumption that both experimental animals and humans

share common basic structure of the body and thus similar biological reaction. Most of those toxicological studies are based on “diagnosis” of the symptoms of experimental animals in a similar fashion to give a diagnosis to human patients. Because the fine structure and function of the bodies are still unknown, both humans and animal bodies are “black boxes” responding to the test substances by showing various symptoms. Usually, the “no observed adverse effect level” (NOAEL) or “no observed effect level” (NOEL) is given by such tests. Since the basic nature of species differences and individual differences are not known, a number called “safety factor” was invented to extrapolate animal NOAEL/NOEL data to humans (Benford, 2000). Normally, a factor of 10 for the species and another 10 for individual differences, thus 100 as a whole, is used to set lower NOAEL/NOEL levels for humans. This approach has been working well for the majority of test substances. Not surprisingly, however, there are some exceptions. Thalidomide is a best-known example (Newman, 1985). Phocomelia, a spectrum of malformation of limbs, was induced in offspring of tha-

Correspondence: Jun Kanno (E-mail: kanno@nihs.go.jp)

lidomide-treated pregnant women, but not observed in offspring of mice and rats. Therefore, more precise toxicity evaluation/prediction is obviously needed for safer assessment. An approach that enables us to point out molecular mechanisms of toxicity would be essential for such needs and to better understand the species-specific responses.

DISCUSSION

To modernize the toxicology and improve the accuracy of safety assessments, we are attempting to describe and understand the organism-xenobiotics interaction at the molecular levels. Different from other exploratory studies, a major prerequisite is that the Toxicology must be prepared for any unexpected or unpredictable responses. Thus, the approach must be comprehensive. Consequently, we adopted a whole-genome cDNA microarray system for a comprehensive monitoring of the transcriptome, and launched the Percellome Toxicogenomics Project, of which the ultimate goal is to illustrate out the whole regulatory pathways induced by xenobiotics in the experimental animals, mainly mice, including embryo (Kanno *et al.*, 2006).

On top of that, there is an important factor of toxicology, that is the "time frame" such as acute, chronic and delayed toxicity. Among them, researches for the assessment of delayed toxicity targeted for children (including fetus and infants) is becoming very important. It is very likely that the children have a chance to be exposed in daily life to a series of substances which can be a cause of delayed toxicity, especially, of the highly evolved systems, that is endocrine, immune and central nervous system. Such chemical substances can affect the developing systems at a dosage lower than the dosage that induces overt cytotoxic changes that would link to immediate appearance of symptoms. For example, our recent experience on the perinatal exposure study (Tanemura *et al.*, 2009) which resulted in the emergence of delayed effects on neurobehavioral endpoints can be explained by a metaphor. That is, "No one turns on power when building a computer, but the living brains are built under the "power-on" situation". It is very likely that the developing brain needs proper or normal signals to build up its fine structures and functional networks (Cohen-Cory, 2002). At this stage, if the signals are disrupted by exogenous insults, it may result in malformation of the fine structure of the brain system. In this case, it is not necessary to directly kill the nerve cells during exposure. The malformation of fine structure/functional network will become symptomatic when the animals grow up to adults. On the

other hand, most of those insults to adults would end up in reversible and transient changes.

Such delayed toxicity cannot be readily detected by currently available functional observational battery-(FOB-) based neuronal test system. Our new findings fall into the category of "early exposure- delayed effect". As mentioned above, nervous systems of developing organisms are susceptible to signal disruption which could lead to the delayed neurobehavioral anomaly. Toxicology is asked to prepare to respond to such new types of toxicity or "signal toxicity" with a consideration on the mechanisms which could explain the severity and irreversibility specific to children.

In conclusion, the 35th Annual Meeting of the Japanese Society of Toxicology had raised "Children's Toxicology" as one of its main Themes, and organized Special lectures, five Symposia and two Workshops on Children's Toxicology of various targets and pending problems, which includes central nervous system, immune system, and endocrine system as targets, as well as problems in pharmacology i.e. issues on children's preclinical and clinical trials and on the off-label use of drugs. This special issue of the Journal of Toxicological Sciences gathers the peer-reviewed papers presented by the authors who participated in the lectures/symposia/workshops on Children's Toxicology at the meeting.

REFERENCES

- Benford, D. (2000): The Acceptable Daily Intake: A food for ensuring food safety. ILSI Europe Concise Monograph series. Brussels, Belgium.
- Cohen-Cory, S. (2002): The developing synapse: construction and modulation of synaptic structures and circuits. *Science*, **298**, 770-776.
- Kanno, J., Aisaki, K., Igarashi, K., Nakatsu, N., Ono, A., Kodama, Y. and Nagao, T. (2006): "Per cell" normalization method for mRNA measurement by quantitative PCR and microarrays. *BMC Genomics*, **7**, 64.
- Newman, C.G.H. (1985): Teratogen update: clinical aspects of thalidomide embryopathy—a continuing preoccupation. *Teratology*, **32**, 133-44.
- Tanemura, K., Igarashi, K., Matsugami, T.R., Aisaki, K., Kitajima, S. and Kanno, J. (2009): Brain structure impairment and behavioral disturbance induced in male mice offspring by a single intraperitoneal administration of domoic acid (DA) to their dams. *J. Toxicol. Sci.*, **34**, Special Issue II, SP279-SP286.

Hypersensitivity of Aryl Hydrocarbon Receptor-Deficient Mice to Lipopolysaccharide-Induced Septic Shock[†]

Hiroki Sekine,^{1,5} Junsei Mimura,^{1,5} Motohiko Oshima,^{1,5} Hiromi Okawa,^{1,5}
Jun Kanno,² Katsuhide Igarashi,² Frank J. Gonzalez,³ Togo Ikuta,⁴
Kaname Kawajiri,⁴ and Yoshiaki Fujii-Kuriyama^{1,5*}

The Center for Tsukuba Advanced Research Alliance and Institute of Basic Medical Sciences, University of Tsukuba, 1-1-1 Tennoudai, Tsukuba 305-8577, Japan¹; Division of Molecular Toxicology, National Institute of Health Sciences, 1-18-1 Kamiyoga, Setagaya-ku, Tokyo 158-8501, Japan²; Laboratory of Metabolism, Center for Cancer Research, National Cancer Institute, National Institutes of Health, Bethesda, Maryland 20892³; Research Institute for Clinical Oncology, Saitama Cancer Center, 818 Komuro, Ina-machi, Kitaadachi-gun, Saitama 362-0806, Japan⁴; and SORST, Japan Science and Technology Agency, 4-1-8 Honcho, Kawaguchi, 332-0012, Japan⁵

Received 16 March 2009/Returned for modification 2 May 2009/Accepted 11 September 2009

Aryl hydrocarbon receptor (AhR), a ligand-activated transcription factor, is known to mediate a wide variety of pharmacological and toxicological effects caused by polycyclic aromatic hydrocarbons. Recent studies have revealed that AhR is involved in the normal development and homeostasis of many organs. Here, we demonstrate that AhR knockout (AhR KO) mice are hypersensitive to lipopolysaccharide (LPS)-induced septic shock, mainly due to the dysfunction of their macrophages. In response to LPS, bone marrow-derived macrophages (BMDM) of AhR KO mice secreted an enhanced amount of interleukin-1 β (IL-1 β). Since the enhanced IL-1 β secretion was suppressed by supplementing Plasminogen activator inhibitor-2 (Pai-2) expression through transduction with Pai-2-expressing adenoviruses, reduced Pai-2 expression could be a cause of the increased IL-1 β secretion by AhR KO mouse BMDM. Analysis of gene expression revealed that AhR directly regulates the expression of Pai-2 through a mechanism involving NF- κ B but not AhR nuclear translocator (Arnt), in an LPS-dependent manner. Together with the result that administration of the AhR ligand 3-methylcholanthrene partially protected mice with wild-type AhR from endotoxin-induced death, these results raise the possibility that an appropriate AhR ligand may be useful for treating patients with inflammatory disorders.

The aryl hydrocarbon receptor (AhR) is a member of the basic helix-loop-helix/Per-Arnt-Sim homology superfamily and is involved in the induction of drug-metabolizing enzymes and the susceptibility of cells to a variety of cytotoxicities induced by dioxins (9). AhR is a ligand-activated transcription factor activated by polycyclic aromatic hydrocarbons (PAHs), such as 3-methylcholanthrene (3MC) and 2',3',7',8'-tetrachlorodibenzo-*p*-dioxin (TCDD). Under normal conditions, AhR exists in the cytoplasm in a complex with Hsp90, XAP2, and p23 (22). After binding a ligand, AhR translocates into the nucleus where it dimerizes with its partner molecule, AhR nuclear translocator (Arnt), and acts as a transcriptional activator to regulate the expression of target genes, such as those expressing drug-metabolizing cytochrome P450 (Cyp1a1, 1a2, and 1b1) and NAD(P)H: quinone oxidoreductase (Nqo), by binding to xenobiotic response element (XRE) sequences in their promoter regions (9). By using AhR knockout (AhR KO) mice, it has been demonstrated that AhR is essential not only for the induction of drug-metabolizing enzymes but also for most, if not all, of the toxicological effects caused by TCDD, including immunosuppression, thymic atrophy, teratogenesis, and hyperplasia (6, 7, 17, 24), the mechanisms for which are largely unknown. Recently, careful investigation into

the loss of functions in AhR KO mice has also revealed that AhR is involved in the normal development of several organs, including the liver, heart, vascular tissues, and reproductive organs (1, 2, 6, 8, 15, 24). In addition, AhR has been found to play a key role in the differentiation of regulatory T cells Treg, Th17, and Th1 from naive CD4 T cells by regulating their expression of Foxp3 or by as-yet-unknown mechanisms (14, 20, 23, 32). From these studies, one of the general features of AhR that begins to emerge is that it serves as a multifunctional regulator in a large number of areas, ranging from drug metabolism to innate immunity for protection against invasive xenobiotics. In the work presented here, we demonstrated that AhR KO mice were hypersensitive to lipopolysaccharide (LPS)-induced septic shock, mainly due to the dysfunction of their macrophages. AhR KO mouse macrophages secreted an enhanced amount of interleukin-1 β (IL-1 β) in response to LPS treatment and had markedly reduced Plasminogen activator inhibitor-2 (Pai-2) mRNA concentrations, as revealed by DNA microarray analysis. Pai-2 was reported to be a negative regulator of IL-1 β secretion through its inhibition of caspase-1 (10), suggesting that the enhanced secretion of IL-1 β by AhR KO macrophages in response to LPS may have been due to the reduced level of Pai-2. We showed that AhR directly regulates the expression of inhibitory Pai-2, in an LPS-dependent manner, through a mechanism involving NF- κ B but not Arnt.

MATERIALS AND METHODS

Mice. AhR knockout (AhR KO) mice were generated as described previously (17). These mice were back-crossed with C57BL/6J mice at least 10 times. Age-matched mice (10 weeks) were intraperitoneally injected with 20 mg of

* Corresponding author. Present address: 5-18-7 Honkomagome, Bunkyo-ku, Tokyo 113-0021, Japan. Phone and fax: 3-3941-2200. E-mail: y.k_fujii@nifty.com.

[†] Supplemental material for this article may be found at <http://mcb.asm.org/>.

[‡] Published ahead of print on 12 October 2009.

LPS/kg of body weight. Mice with floxed *Arnt* (30) and *AhR* (Jackson laboratory) alleles were crossed to LysM Cre mice to specifically delete these genes in their macrophages. *AhR^{fllox/-}* and *AhR^{fllox/-}::LysM Cre* mice were generated by mating *AhR^{fllox/fllox}::LysM Cre* and *AhR^{-/-}* (*AhR KO*) mice. These age-matched mice (9 to 11 weeks old) were intraperitoneally injected with 25 mg LPS/kg. Mouse survival was checked every 6 or 12 h. 3MC (Wako, Osaka) at 10 μ l (4 mg/ml 3MC/g of body weight or 10 μ l corn oil/g was intraperitoneally injected. After 2 h, each mouse was intraperitoneally injected with 30 mg LPS/kg. LPS (from *Escherichia coli* 0111:B4) was purchased from Sigma.

Preparation of macrophages. Bone marrow cells were obtained from the femurs of 8- to 12-week-old mice. The bone marrow-derived macrophages (BMDM) used for each experiment were isolated by culturing bone marrow cells in the presence of 10 ng/ml granulocyte-macrophage colony-stimulating factor (PeproTech) for 7 days and washing the attached cells with phosphate-buffered saline (PBS) three times. For cytokine assays, washed cells were collected with a scraper, plated at 2×10^6 cells/ml in 96-well plates, and cultured with 10 ng/ml LPS for 8 h.

For isolation of peritoneal exudate macrophages (PEMs), mice were intraperitoneally injected with 2 ml of 4% thioglycolate. Peritoneal cells were isolated from exudates of the peritoneal cavity 3 days after injection, incubated for 3 h in appropriate plates, and washed with PBS. The adherent cells were used for experiments.

Measurement of cytokines. Mice were intraperitoneally injected with 20 mg/kg LPS and bled 2 h after injection. Plasma concentrations of IL-1 β , tumor necrosis factor alpha (TNF- α), IL-6, gamma interferon (IFN- γ), IL-12, and IL-18 were determined by enzyme-linked immunosorbent assay (ELISA) (Biosource). BMDM of mice with wild-type *AhR* (*AhR WT* mice) and *AhR KO* at 2×10^6 cells/ml were incubated with 10 ng/ml LPS for 8 h, and their culture supernatants were assessed for cytokines using mouse TNF- α and IL-1 β ELISAs (Biosource).

Cell culture. All cells were maintained in RPMI medium (Sigma) supplemented with 10% fetal bovine serum (HyClone) and penicillin/streptomycin (Gibco) under 5.0% CO₂ at 37°C.

Caspase inhibitors. BMDM of *AhR KO* mice at 2×10^6 cells/ml were incubated with dimethyl sulfoxide (DMSO) or 80 μ M Z-YVAD-FMK (caspase-1 inhibitor VI; Merck) or 100 μ M Z-VAD-FMK (caspase inhibitor VI; Merck) for 30 min before LPS (10 ng/ml) stimulation. The BMDM were incubated for 8 h, and their culture supernatants were assessed for cytokines using a mouse IL-1 β ELISA (Biosource).

Virus infections. Adenoviruses expressing green fluorescent protein (GFP), human Pai-2 (hPai-2), and human Bcl-2 (hBcl-2) were purchased from Vector Biolabs (Philadelphia). BMDM from *AhR KO* mice were infected for 12 h with adenoviruses expressing GFP, hPai-2, and hBcl-2 at a multiplicity of infection of 100. Infected BMDM were washed with PBS, followed by 12 h of incubation. As it was reported that adenoviral vectors enhanced IL-1 β secretion in macrophages (19), IL-1 β levels were investigated in these incubation supernatants by ELISA. At this point, no IL-1 β was observed in the supernatants. Therefore, the cells were washed, collected with a scraper, and plated at 2×10^6 cells/ml in 96-well plates. The cells were treated with 10 ng/ml of LPS for an additional 8 h.

Retroviral infection was performed as follows: pQC-mAhR, a cloned murine *AhR* (mAhR) fragment in pQCXIN (Clontech), and pQCXLN for LacZ expression (as a control) were transfected into PT67 cells that were then cultured for 24 h. The culture medium was replaced with fresh medium, and the culture was continued for an additional 24 h. This culture medium was used as the retrovirus particle source.

Microarray analysis. Total RNA samples were purified using Isogen before being processed and hybridized to Affymetrix mouse genome 430 2.0 arrays (Affymetrix). The experimental procedures for the GeneChip analyses were performed according to the Affymetrix technical manual.

Generation of stable transformant cell lines. ANA-1 cells were the kind gift of L. Varesio (3). ANA-1 cells were transduced with LacZ- or *AhR*-expressing retroviruses in a suspension with 8 mg/ml of Polybrene. One day after infection, the infected cells were replated and incubated in a selection medium containing 0.5 mg/ml of Geneticin (Gibco).

Plasmids. pcDNA3-p65 and pcDNA3-AhR were generated by inserting *AhR* and p65 cDNA fragments, excised from pBS-mAhR and pBS-mp65 (murine p65), into the pcDNA3 vector. The 2.7-kb fragment upstream of the Pai-2 transcription start site was generated by PCR (primers 5'-gaagcttGGGTTGCA GATCCCTTAGC-3' and 5'-ccatgggCTGACACACAGAAATGCTTC-3'; lowercase indicates restriction site sequences for cloning), using a BAC vector carrying the Pai-2 gene as a template, and then cloned into the pBS vector. After sequencing, the construct was cleaved with *I*IndIII/*N*coI, and the isolated insert was cloned into the HindIII/*N*coI-digested pGL4.10 (Promega) to produce pGL4-Pai-2 (-2.7 kb). The 0.8-kb fragment upstream of the Pai-2 transcription

start site was generated by PCR (primers 5'-ggaattcGAGAAGTGTCTGGTA GATG-3' and 5'-ccatgggCTGACACACAGAAATGCTTC-3') using pGL4-Pai-2 (-2.7 kb) as a template and cloned into the pBS vector. After sequencing, the construct was cleaved with HindIII/*N*coI, and the isolated insert was cloned into the HindIII/*N*coI-digested pGL4.10 (Promega) to produce pGL4-Pai-2 (-0.8 kb). pGL4-Pai-2 (-0.55 kb) was produced by cleaving pGL4-Pai-2 (-2.7 kb) with *N*deI/*E*coRV. pGL4-Pai-2 (-0.1 kb) was generated in a similar manner, using primers 5'-GATGCTTTATGAGTAAATGTTGAATCA-3' and 5'-cca tggggCTGACACACAGAAATGCTTC-3'. pGL4-Pai-2 (-0.55 kb C/EBP β mutant) was generated by site-directed mutagenesis using a Sculptor in vitro mutagenesis system (Amersham) with pGL4-Pai-2 (-0.55 kb) as a template and primer pair 5'-GATTTAAAATTTGGAAAGGCTAAATTCCTGAATTTTGAA TGACATCAC-3' and 5'-GTGATGTTCATCAAAATTCAGAAATTTAGCcc TTTCCAATTTTAAATC-3'.

RNA preparation and reverse transcription PCR (RT-PCR). Total RNA was prepared using Isogen (Nippon Gene, Tokyo) according to the manufacturer's protocol. cDNA synthesis from 1 μ g of total RNA was carried out using SuperScript II reverse transcriptase (Invitrogen, United States). Real-time PCR was performed using an ABI7300 real-time PCR system (Applied Biosystems) and Platinum SYBR green quantitative PCR SuperMix (Invitrogen, United States). Each sample was normalized to the expression of β -actin as a control. The primer sequences were as follows: Pai-2, 5'-GCATCCACIGGCTTGGAA-3' and 5'-GGGAATGTAGACCAACATCAT-3'; Bcl-2, 5'-GTGGTGGAGGA ACTCTTCAGGGATG-3' and 5'-GGTCTTCAGAGACGCCAGGAGAAAT C-3'; AhR, 5'-TTCTATGCTTCCTCCATCA-3' and 5'-GGCTTCGTCC ACTCTTGT-3'; Arnt, 5'-GGACGGTCCATCTCGAC-3' and 5'-CATCTG GTCATCATCGCATC-3'; Mmp-8, 5'-CCACACACAGCTTGCCAAATGCC T-3' and 5'-GGTCAGGTTAGTGTGTGTCAC-3'; Nqo1, 5'-TTAGGGTC GTCTTGGCAAC-3' and 5'-AGTCAAATCAGGGCTCTCTCC-3'; AhR repressor, 5'-CCTGTCCCGGGATCAAAGATG-3' and 5'-CTCACACCAG AGCGAAGCCATTGA-3'; IL-1 β , 5'-CTGAAGCAGCTATGGCAACT-3' and 5'-GGATGCTCTCATCTGGACAG-3'; TNF- α , 5'-CTGTAGCCCAAGCTCGT AGC-3' and 5'-TTGAGATCCATGCGGTTG-3'; Cox-2, 5'-GCATCTTTGCC CAGCACIT-3' and 5'-AGACCAGGCCACAGACCAAAAG-3'; β -actin, 5'-GA CAGGATCCAGAGGAGAT-3' and 5'-TTGCTGATCCACATCTGCTG-3'; hPai-2, 5'-CCAGAACCTCTTCTCTCC-3' and 5'-CATTGGCTCCACIT CATT-3'; and hBcl-2, 5'-GTGTGTGGAGAGCGTCAACC-3' and 5'-GAGA CAGCCAGGAGAAATCAA-3'.

Reporter assays. All luciferase assays were performed using a dual-luciferase reporter assay system according to the manufacturer's protocol (Promega), with some modifications. RAW 264.7 cells (2.0×10^4 cells/well) were plated in 24-well plates 24 h prior to transfection. Cells were cotransfected with 100 ng pGL4-Pai-2 (various lengths in kilobases) (see "Plasmids"), 1 ng *Renilla* luciferase (as an internal control), and 1 ng pcDNA3-p65 and/or pcDNA3-AhR using FuGENE HD transfection reagent (Roche) according to the manufacturer's protocol. All cells were incubated for 12 h at 37°C after transfection, treated with 10 ng/ml LPS, and incubated for an additional 6 h.

Co-IP assays. *AhR WT* PEMs or transfected 293T cells were washed with ice-cold PBS, followed by buffer containing 20 mM HEPES, pH 7.4, 125 mM NaCl, 1% Triton X-100, 10 mM EDTA, 2 mM EGTA, 2 mM Na₂VO₄, 50 mM sodium fluoride, 20 mM ZnCl₂, 10 mM sodium pyrophosphate (31). The cells were harvested by scraping, centrifuged at 5,000 rpm at 4°C for 5 min, and suspended in immunoprecipitation (IP) buffer containing a protease inhibitor cocktail (Roche). The cells were vortexed and placed on ice for 10 min. The samples were then centrifuged at 15,000 rpm for 5 min at 4°C, and the supernatants were saved as whole-cell lysates.

The prepared whole-cell lysate (250 μ l) was incubated with anti-immunoglobulin G, anti-AhR antibody, or anti-p65 for 2 h at 4°C. The reaction mixture was supplemented with 20 μ l of protein A-agarose beads (Amersham). After being incubated for an additional 1 h at 4°C, the beads were washed three times with IP buffer containing protease inhibitor cocktail and resuspended in sodium dodecyl sulfate (SDS) sample buffer. The coimmunoprecipitated proteins were resolved by SDS-polyacrylamide gel electrophoresis (PAGE), and Western blot analysis was performed.

ChIP assays. Chromatin IP (ChIP) assays were performed with PEMs from *AhR WT* and *AhR KO* mice. PEMs were stimulated with 10 ng/ml LPS for 60 min and then fixed with formaldehyde for 10 min. The cells were lysed and sheared by sonication. The lysis solution was incubated with immunoglobulin G or preimmune serum and protein A-agarose for 2 h to remove nonspecific DNA binding. The solution was incubated overnight with a specific antibody, followed by incubation with protein A-agarose saturated with salmon sperm DNA. Precipitated DNA was analyzed by real-time PCR using primer pair 5'-GGAAGT TCCCTGAGGCTTATAGG-3' and 5'-ATGGAAGCACATACATAAGAACA

TGG-3' for the NF- κ B binding site of Pai-2, 5'-TGAGTGTGAGTGTGTCAG ATTAC-3' and 5'-CCTCCCACACAGCTCTTTTTC-3' for mPai-2 TATA, 5'-CGGAGGGTAGTTCATGAAA-3' and 5'-CAGGCTTTTACCCACGCAA A-3' for the NF- κ B binding site of mCox2, and 5'-CGCAACTCACTGAAGC AGAG-3' and 5'-TCCTTCGTGAGCAGAGTCCT-3' for mCox-2 TATA. The antibodies used were as follows: anti-AhR serum, preimmune serum, anti-p65, and anti-PolIII antibodies (Santa Cruz).

Western blot analyses. Cells were dissolved in SDS sample buffer, and proteins were separated by SDS-PAGE for Western blot analysis. The proteins were then transferred to polyvinylidene difluoride membranes and blocked in 3% skim milk for 30 min. Each antibody was used as a primary reagent, and after being washed three times with Tris-borate-EDTA containing 0.1% Triton X-100, membranes were incubated with species-specific horseradish peroxidase-conjugated secondary antibody (Zymed). The protein-antibody complexes were visualized by using an enhanced chemiluminescence detection system (Amersham) according to the manufacturer's recommendations. Nuclear extracts were prepared by a standard method (25). The antibodies used were as follows: anti-Arnt serum (28); anti-AhR (Biomol); anti-Pai-2, anti-p65, and antilamin antibodies (Santa Cruz); and antitubulin antibody (Sigma).

RESULTS

High susceptibility of AhR-deficient mice to LPS-induced endotoxin shock. To investigate the function of AhR in acute inflammation *in vivo*, we performed studies of experimental LPS-induced endotoxin shock. For these studies, 10-week-old AhR WT and AhR KO mice were injected intraperitoneally with 20 mg/kg LPS. After 24 h, while all of the AhR WT mice survived, most of the AhR KO mice (80%) had died (Fig. 1A). These data indicate that AhR-deficient mice were highly susceptible to LPS-induced endotoxin shock. To explain the increased sensitivity of AhR KO mice to septic shock, the plasma concentrations of several inflammatory cytokines were measured 2 h after LPS challenge. Consistent with the enhanced susceptibility of AhR KO mice to the LPS treatment, AhR KO mice had marked increases in plasma IL-1 β , IL-18, and TNF- α levels ($P < 0.001$), with modest increases in IL-6 and IFN- γ (Fig. 1B). In contrast, there was no difference in plasma IL-12p70 levels (Fig. 1B). Administration of 3MC, an AhR ligand, before LPS treatment (30 mg/kg) made the AhR WT mice significantly more resistant to septic shock than the mice that were not treated with 3MC ($P = 0.002$) (Fig. 1C). Together with the fact that there was essentially no effect of 3MC on AhR KO mice, these results suggested that activated AhR could play an anti-inflammatory role.

Increased susceptibility of mice with AhR KO macrophages to LPS-induced endotoxin shock. Since macrophages play an important role in sensitivity to LPS toxicity, we generated mice with macrophages deficient in AhR (AhR^{fllox/-}::LysM Cre [Δ AhR Mac] mice) to evaluate the contribution of macrophages to the LPS hypersensitivity of AhR KO mice. When Δ AhR Mac and control mice (AhR^{fllox/-}) were injected intraperitoneally with 25 mg/kg LPS, most of the Δ AhR Mac mice (80%) had died at 48 h after LPS challenge, while 60% of the control mice survived ($P = 0.03$) (Fig. 2A). Together with the previous results, these data showed that dysfunctional AhR-deficient macrophages are one of the main causes of LPS hypersensitivity in AhR KO mice.

Elevated IL-1 β secretion from AhR KO BMDM in response to LPS. To further investigate the cause of the aberrant cytokine secretion by LPS-challenged AhR KO mice, we next asked if there were any differences in the production of proinflammatory cytokines by AhR WT and AhR KO mouse

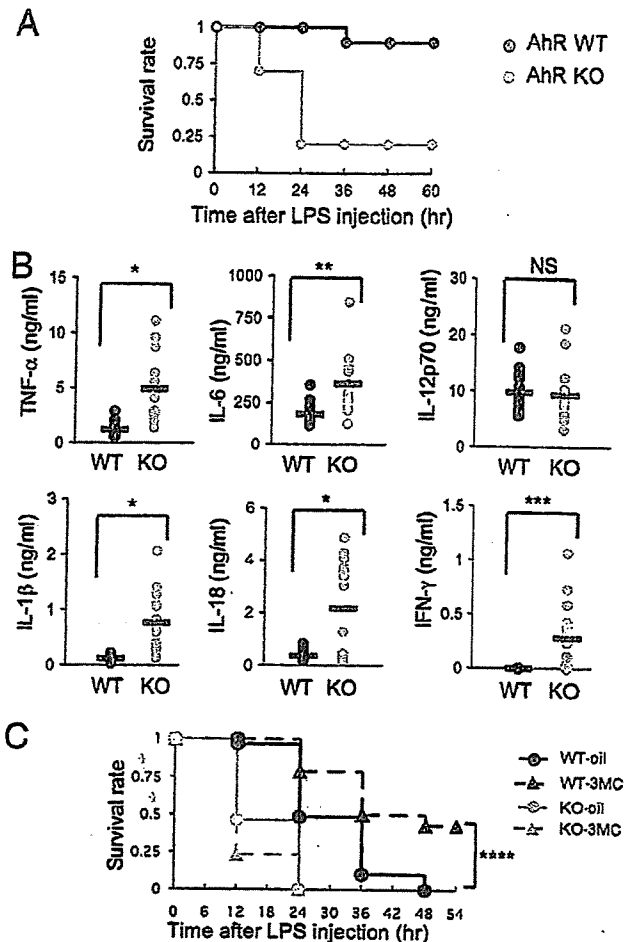


FIG. 1. High susceptibility of AhR KO mice to LPS-induced endotoxin shock. (A) Survival of AhR WT and AhR KO mice ($n = 10$) after LPS challenge (20 mg/ml). (B) TNF- α , IL-6, IL-12p70, IL-1 β , IL-18, and IFN- γ plasma levels 2 h after LPS challenge (20 mg/ml). Horizontal bars show the mean results. (C) Partial protection of AhR WT mice from septic shock by intraperitoneal injection of 3MC at 2 h before LPS challenge (30 mg/ml) and survival of corn oil-injected mice. AhR WT-oil, $n = 29$; AhR WT-3MC, $n = 28$; AhR KO-oil, $n = 13$; AhR KO-3MC, $n = 13$. *, $P < 0.001$; **, $P = 0.001$; ***, $P < 0.005$; ****, $P = 0.002$; NS, not significant.

BMDM in response to LPS stimulation. Macrophages from the bone marrow of AhR WT and AhR KO mice were challenged with 10 ng/ml LPS for 8 h, and then the levels of TNF- α and IL-1 β in the culture medium were assessed by ELISA. Compared to the levels in AhR WT BMDM, the levels of IL-1 β secretion by AhR KO BMDM were markedly elevated, along with slight increases in TNF- α , in response to LPS treatment ($P < 0.001$) (Fig. 2B, left). However, IL-1 β mRNA levels were not altered between AhR WT and AhR KO BMDM (Fig. 2C, left). These data indicated that AhR deficiency markedly increased IL-1 β accumulation due to its enhanced secretion rather than its increased synthesis.

Expression of AhR-dependent genes in macrophages. We next performed microarray analysis of AhR WT and AhR KO mouse macrophages to comprehensively investigate the AhR-

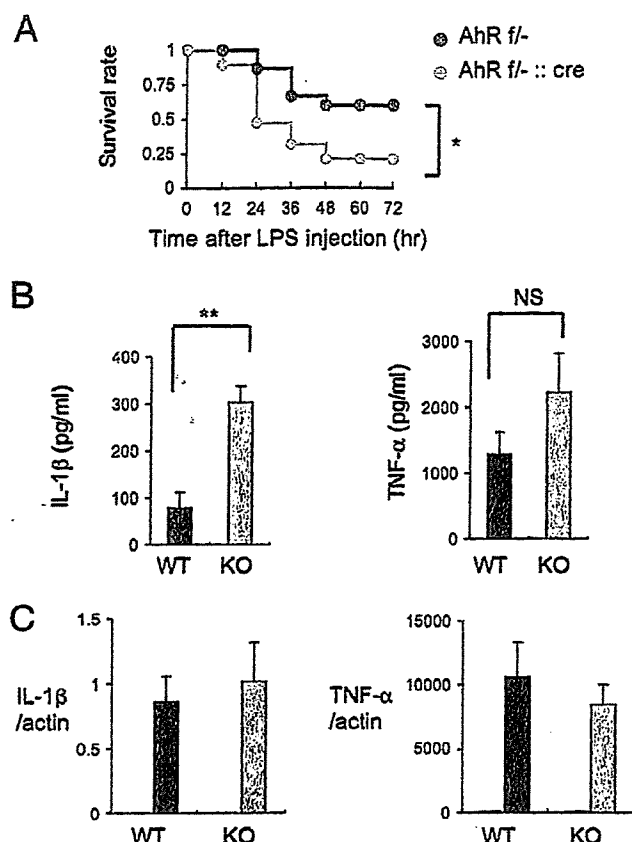


FIG. 2. LPS induces abnormal secretion of IL-1 β by BMDM from AhR KO mice. (A) Survival of AhR^{fl/-} (AhR *fl/-*; $n = 15$) and AhR^{fl/-::LysM Cre} (AhR *fl/-::cre*; $n = 19$) mice after LPS challenge (25 mg/ml). (B) IL-1 β and TNF- α levels in the culture supernatants of AhR WT and AhR KO BMDM 8 h after LPS stimulation (10 ng/ml) ($n = 4$). (C) Relative expression levels of IL-1 β and TNF- α mRNA 4 h after LPS stimulation (10 ng/ml) of AhR WT and AhR KO BMDM. Gray and black bars show results with LPS; white bars show results for untreated cells. Error bars show standard deviations. *, $P = 0.03$; **, $P < 0.001$; NS, not significant.

dependent changes in gene expression that were related to IL-1 β secretion (Table 1). Among the genes whose expression was reduced in AhR KO macrophages, we noted the markedly reduced levels of expression of the *Pai-2* and *Bcl-2* genes.

These genes were significant because they had been reported to negatively regulate IL-1 β secretion by inhibiting the activity of caspase-1 (5, 10). Consistent with the notion that the enhanced secretion of IL-1 β is due to the activation of caspase-1, treatment with the caspase inhibitors Z-YVAD-FMK and Z-VAD-FMK markedly reduced the secretion of IL-1 β in AhR KO BMDM (Fig. 3A). To confirm their reduced expression in AhR KO BMDM, *Pai-2* and *Bcl-2* mRNA expression levels were determined by real-time RT-PCR in AhR WT and AhR KO BMDM (Fig. 3B). Figure 3B shows that *Pai-2* and *Bcl-2* mRNA expression levels were clearly reduced in AhR KO BMDM. To investigate whether the increased IL-1 β secretion in AhR KO BMDM was due to their reduced *Pai-2* and *Bcl-2* expression, the expression of these proteins was supplemented in AhR KO BMDM by infection with adenoviral vectors expressing h*Pai-2* and h*Bcl-2* (Fig. 3D). The efficiency of the adenoviral gene transfer, as monitored by the expression of GFP, was estimated to be >90% (data not shown). Compared with control adenoviral expression of GFP, transfer of the h*Pai-2* gene into AhR KO BMDM significantly inhibited LPS-induced secretion of IL-1 β (Fig. 3C), but almost no effect was observed with *Bcl-2* expression. *Bcl-2* has been reported to suppress IL-1 β secretion that is specifically processed through the NALP1 complex and regulated by muramyl dipeptide, which is usually a contaminant in commercial LPS (5). These results suggested that the enhanced IL-1 β secretion in response to LPS was due not to processing through the NALP1 complex (5) but to processing through the NALP3 complex, an inflammasome-containing caspase-1 regulated by LPS (16), and that decreased *Pai-2* expression is at least one of the causes for the increased IL-1 β secretion by AhR KO BMDM after LPS treatment.

Arnt is not required for enhancement of LPS-induced *Pai-2* expression by AhR. It has been reported that LPS stimulation induces *Pai-2* expression (21, 26). Figure 4A and B show that the induction of both *Pai-2* mRNA and protein expression was remarkably reduced in AhR KO macrophages compared with the levels in AhR WT macrophages. Interestingly, AhR mRNA and protein expression levels were also induced by LPS stimulation (Fig. 4A and B). In response to various PAHs, AhR is known to act, in most cases, as a transcriptional activator, in heterodimer formation with Arnt. Although the mouse *Pai-2* promoter does not have any obvious XRE sequences (GCGTG) in its regions 5 kb upstream and down-

TABLE 1. Decreased gene expression in AhR KO PEMs revealed by cDNA microarray analysis

Fold change	Value for		Gene name	Gene product
	WT PEMs	KO PEMs		
14.0	0.561	0.040	<i>Gsta3</i>	Glutathione S-transferase alpha 3
10.2	7.826	0.767	<i>Pai-2</i>	Plasminogen activator inhibitor-2
5.5	9.354	1.700	<i>Cyp1b1</i>	Cytochrome P450, family 1, subfamily b, polypeptide 1
4.6	0.206	0.045	<i>Nfya</i>	NF- κ B repressing factor
3.6	1.922	0.541	<i>Cxcl5</i>	Chemokine (C-X-C motif) ligand 5
3.1	13.670	4.444	<i>Mmp8</i>	Matrix metalloproteinase 8
2.9	1.406	0.489	<i>Cxcl13</i>	Chemokine (C-X-C motif) ligand 13
2.6	2.111	0.800	<i>Lrrc27</i>	Leucine-rich repeat-containing 27
2.5	3.466434	1.394728	<i>Ctgf</i>	Connective tissue growth factor
2.2	3.849141	1.722473	<i>Mcoln3</i>	Mucopolipin 3
2.2	1.204793	0.550093	<i>Nqo1</i>	NAD(P)H dehydrogenase, quinone 1
2.0	6.96623	3.453017	<i>Irf3</i>	Immediate early response 3
2.0	0.596479	0.294062	<i>Bcl2</i>	B-cell leukemia/lymphoma 2

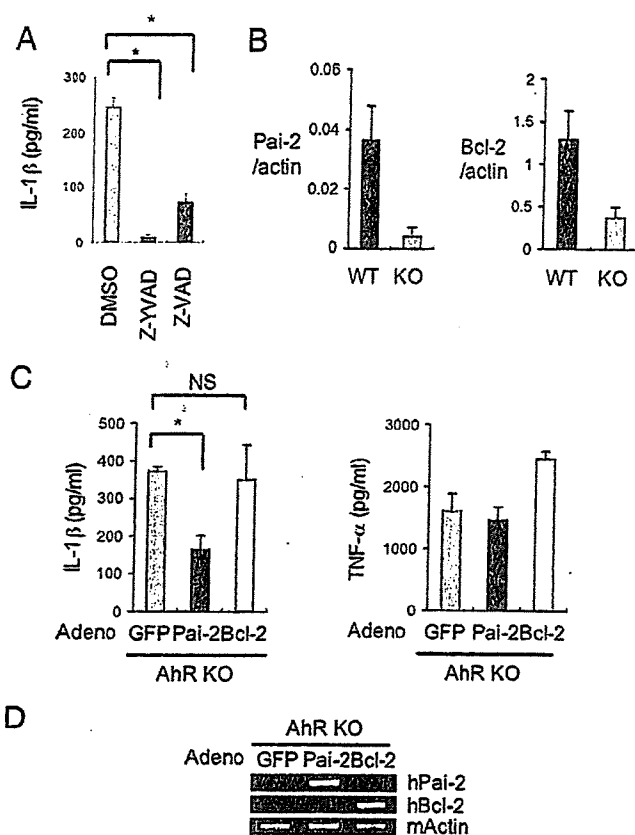


FIG. 3. Decreased Pai-2 expression is one of the causes of the increased IL-1 β secretion by LPS-treated AhR KO BMDM. (A) Inhibition of IL-1 β oversecretion from AhR KO BMDM by treatment with caspase-1 inhibitor (Z-VAD-FMK) or caspase inhibitor (Z-VAD-FMK). (B) Relative expression levels of Pai-2 and Bcl-2 mRNA in AhR WT and AhR KO BMDM. (C) The effect of hPai-2 and hBcl-2 reconstitution on the LPS-induced secretion of IL-1 β and TNF- α by AhR KO BMDM. BMDM from AhR KO mice were infected with the individual adenovirus (adeno) vectors and then washed and incubated for 24 h. IL-1 β and TNF- α levels in the supernatants 8 h after LPS stimulation ($n = 3$) were determined by ELISA. (D) Assessment of hPai-2 and hBcl-2 mRNA expression in adenovirus (adeno) vector-infected BMDM by conventional RT-PCR. Error bars show standard deviations. *, $P < 0.001$; NS, not significant.

stream of the transcription start site, we were interested in determining whether Arnt was also involved in the inducible expression of Pai-2 by LPS. Other AhR target genes identified by the microarray analysis, e.g., the matrix metalloproteinase (Mmp-8) gene and the NAD(P)H:quinone oxidoreductase 1 (Nqo1) gene (Table 1), have characteristic XRE sequences in their promoter regions and were also induced by 3MC. As expected, the induction of their expression was greatly reduced in Arnt KO and Arnt small interfering RNA (siRNA)-treated macrophages (Fig. 4E; also see Fig. S1 in the supplemental material). In stark contrast, the expression of Pai-2 was not much different in Arnt KO and Arnt siRNA-treated macrophages, indicating that Arnt is not involved in regulating Pai-2 gene expression (Fig. 4D; also see Fig. S1 in the supplemental material) and that AhR regulates Pai-2 gene expression by a noncanonical mechanism. Consistent with these observations,

macrophage-specific conditional deletion of Arnt did not significantly alter the sensitivity to LPS treatment (Fig. 4F).

DNA elements regulating Pai-2 gene expression. We were interested in further investigating how AhR regulates Pai-2 gene expression in macrophages. It has been previously reported that LPS-induced Pai-2 expression requires NF- κ B activation (21) and that AhR and p65 physically interact with each other (31). With those results in mind, we constructed a reporter gene by fusing a 2.7-kb sequence upstream of the mouse Pai-2 transcription start site to the luciferase gene (see Fig. S2 in the supplemental material). This 2.7-kb Pai-2 reporter gene contained a previously reported NF- κ B site (21). When the AhR expression vector alone was transfected into RAW 264.7 cells, it did not enhance LPS-induced reporter gene expression. In contrast, cotransfection of both AhR and p65 did (Fig. 5A). To identify the sequence responsible for enhancing the LPS-induced activation of the reporter gene, we constructed an 0.8-kb Pai-2 reporter gene by deleting the sequence from -2.7 to -0.8 kb, which contained the previously reported NF- κ B site (see Fig. S2 in the supplemental material). With this 0.8-kb Pai-2 construct, the addition of AhR and p65 no longer enhanced the activity in response to LPS treatment (Fig. 5A), indicating that the sequence between -0.8 and -2.7 kb, containing an NF- κ B site, is responsible for enhancing Pai-2 gene activation in response to AhR and NF- κ B. Further downstream, we noticed the presence of a putative C/EBP β binding sequence (around 250 base pairs upstream of the transcription initiation site), which has been reported to be responsible for LPS-induced activation of the gene (4). Deletion or point mutation of this sequence was found to abrogate the ability of LPS to induce this gene, indicating that this C/EBP β binding site functions as an enhancer sequence in the LPS response (see Fig. S2 in the supplemental material).

Recruitment of transcription factors necessary for LPS-induced Pai-2 expression. When macrophages were treated with LPS, p65 translocated from the cytoplasm into the nucleus independently of AhR (Fig. 5B), as reported previously. However, without AhR, ChIP revealed that p65 was not recruited to the enhancer sequence in the Pai-2 gene, which contains an NF- κ B site (Fig. 5E). In WT macrophages, nuclear-translocated p65 was only recruited to the enhancer sequence of the Pai-2 gene together with AhR. PolII was concomitantly recruited to the TATA sequence of the Pai-2 gene in AhR WT but not AhR KO macrophages. Surprisingly, we observed that LPS induced AhR binding to the Pai-2 NF- κ B site, as shown by ChIP using an anti-AhR antiserum. Co-IP assays revealed that AhR and p65 interacted in macrophages (Fig. 5C), consistent with a previous report (31). On the other hand, expression of the Cox-2 gene is known to be activated by LPS through recruitment of p65 to its NF- κ B binding site, and this occurs independent of AhR (Fig. 5D), with concomitant binding of PolII to the transcription initiation site (TATA) of the Cox-2 gene (Fig. 5E). Arnt was not recruited to the Pai-2 promoter by ChIP assay (data not shown), consistent with normal Pai-2 expression in the macrophages from Arnt^{fllox}; Δ LysM Cre mice (Fig. 4D).

As shown in Fig. S3 in the supplemental material, the CCAAT box sequence in the Pai-2 gene was recognized by C/EBP β in an LPS-dependent manner in both AhR WT and KO macrophages. This binding of C/EBP β to the Pai-2 pro-

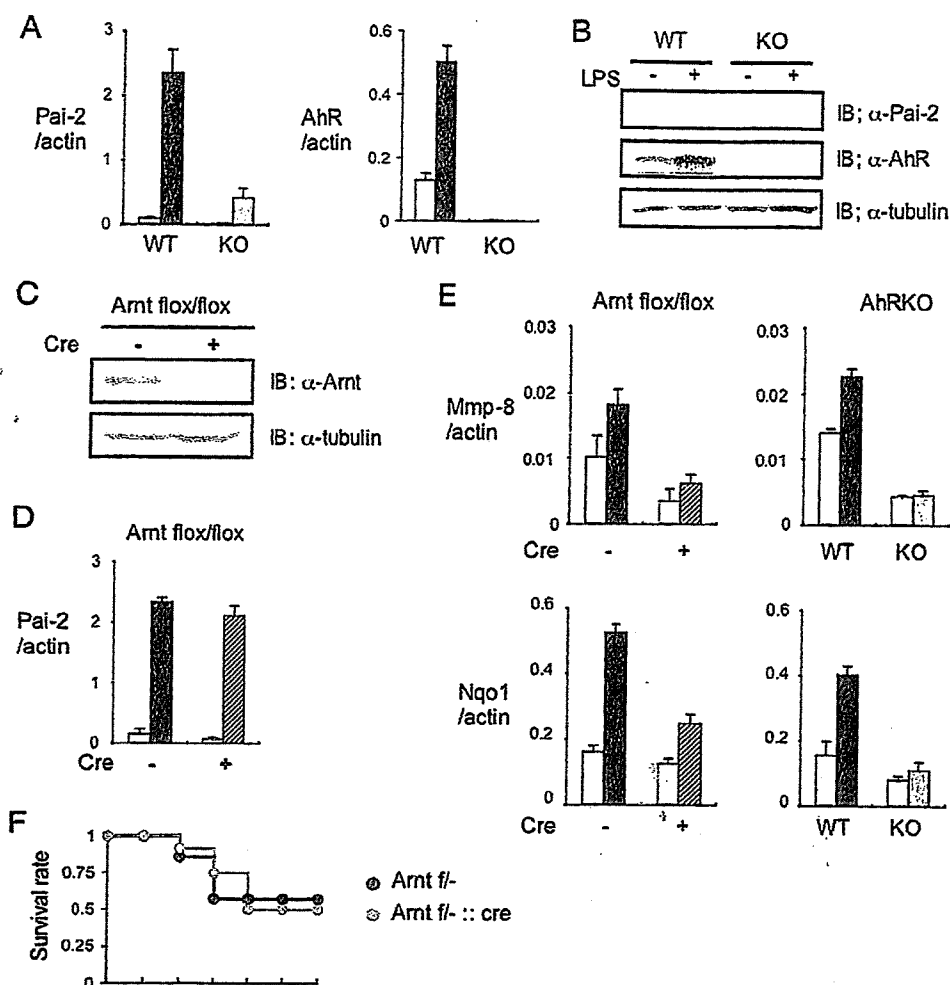


FIG. 4. Arnt is not required for LPS-induced enhancement of Pai-2 expression. (A) Relative Pai-2 and AhR mRNA expression levels in AhR WT and AhR KO PEMs 4 h after treatment with (black or gray bars) or without (white bars) LPS (10 ng/ml). (B) Immunoblot analysis of Pai-2 and AhR expression in AhR WT and KO PEMs after a 16-h incubation with LPS (10 ng/ml). (C) Immunoblot analysis of Arnt in Arnt^{flox/flox} and Arnt^{flox/flox}::LysM Cre PEMs. (D) Relative Pai-2 mRNA expression levels 4 h after incubation of Arnt^{flox/flox} (black bar) and Arnt^{flox/flox}::LysM Cre (hatched bar) PEMs with LPS (10 ng/ml). (E) Left, relative expression levels of Mmp-8 and Nqo1 mRNA in Arnt^{flox/flox} (black bar) and Arnt^{flox/flox}::LysM Cre (hatched bar) PEMs treated with DMSO (white bars) or 3MC (black or hatched bar) (1 μ M). Right, relative expression levels of Mmp-8 and Nqo1 mRNA in AhR WT (black bar) and AhR KO (gray bar) PEMs treated with DMSO (white bars) or 3MC (black or gray bar) (1 μ M). (F) Survival of Arnt^{flox/flox} (Arnt^{flox/flox}; $n = 7$) and Arnt^{flox/flox}::LysM Cre (Arnt^{flox/flox}::LysM Cre; $n = 12$) mice after LPS challenge (25 ng/ml). Error bars show standard deviations. IB, immunoblot; +, present; -, absent; α , anti.

motor might explain the weak LPS-induced activation of Pai-2 gene expression in AhR KO macrophages (Fig. 4A; also see Fig. S3 in the supplemental material), as described in the previous section.

The requirement of the functional domains of AhR for AhR-dependent Pai-2 expression. To determine the functional domains of AhR for AhR-dependent Pai-2 expression, we investigated the Pai-2 expression in ANA-1 cells, which were transfected with various AhR mutants (Fig. 6). Compared with the levels in ANA-1 cells transfected with full-length AhR, we observed much lower levels of expression of Pai-2 in the ANA-1 cells transfected with AhR NLSm (a mutant located predominantly in the cytoplasm) (Fig. 6B, bars 3, 4, 11, and 12). On the other hand, transfection with AhR CA (a consti-

tutively active mutant located predominantly in the nucleus) gave a result for Pai-2 expression comparable to that of the transfection with full-length AhR (Fig. 6B, bars 3, 4, 7, and 8). These results indicated that nuclear AhR functions in AhR-dependent Pai-2 expression. The fractionation of AhR indicated that a small but significant amount of AhR existed in the nucleus without treatment with ligands such as 3MC, in contrast with the large amount in the cytoplasm (Fig. 5B), consistent with the previous report that AhR has functional nuclear localization signal and nuclear export signal sequences and shuttles between the cytoplasm and nucleus. It is reported that when nuclear export is inhibited by trichomycin B or phosphorylation at S68, AhR accumulates in the nucleus (12). Therefore, it could be considered that in macrophages, AhR is in-

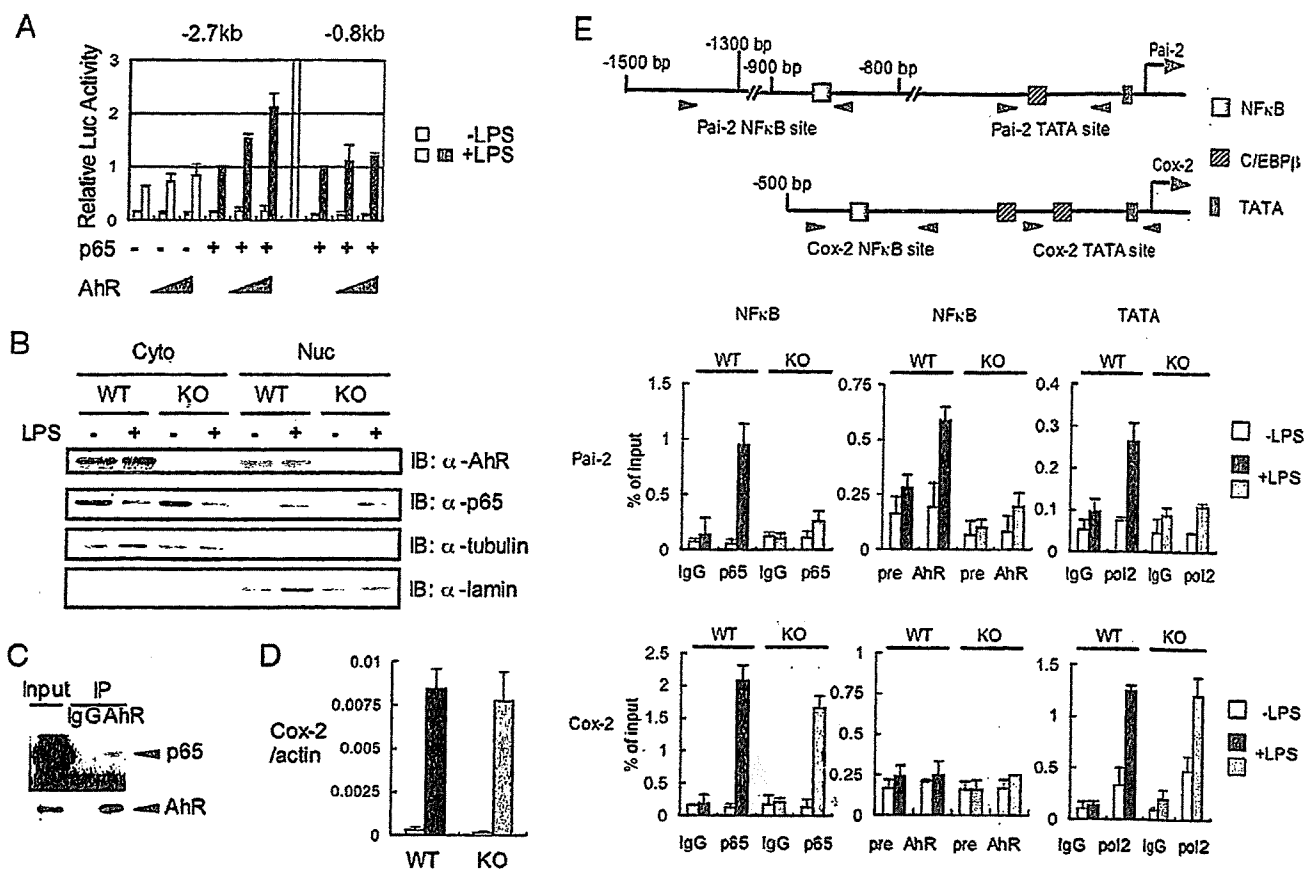


FIG. 5. Recruitment of transcription factors necessary for LPS-induced Pai-2 expression. (A) LPS-induced luciferase expression from the Pai-2 (-2.7 kb) and Pai-2 (-0.8 kb) reporter genes. RAW 264.7 cells were transfected with each reporter gene, with and without pcDNA3-AhR (0 ng, 50 ng, 100 ng) and/or pcDNA3-p65 (1 ng). Values represent the means, normalized to *Renilla* luciferase activity (used as an internal control), \pm standard deviations of the results of three independent experiments. The activities shown by the fourth and seventh pairs of bars were used as standards for normalizing the relative activities of the other conditions. (B) AhR WT and AhR KO PEMs were left untreated or were treated with LPS for 1 h. Cytoplasmic (Cyto) and nuclear (Nuc) extracts were immunoblotted with antibodies against AhR, p65, tubulin, and lamin. (C) Co-IP of AhR and p65. Whole-cell extracts from AhR WT PEMs were coimmunoprecipitated with anti-AhR antibody. Co-IPs and Western blotting were performed as described in Materials and Methods. (D) Relative expression levels of Cox-2 mRNA in AhR WT and AhR KO PEMs after 4 h of treatment with or without LPS (10 ng/ml). Bars are as labeled in panel A. Error bars show standard deviations. (E) Top, transcription factor binding sites in the Pai-2 and Cox-2 genes. Bottom, results of ChIP analyses of the Pai-2 and Cox-2 promoters. ChIP analyses were performed using antibodies to p65, AhR, and PolII in LPS-induced AhR WT and AhR KO PEMs. ChIP analyses and real-time PCRs were performed as described in Materials and Methods. Error bars show standard deviations. +, present; -, absent; α , anti; IgG, immunoglobulin G.

involved in Pai-2 expression induced by LPS treatment in the absence of typical AhR ligands (Fig. 4A). The mechanism of AhR's involvement in Pai-2 expression induced by LPS will be investigated in detail. To further address the question of the requirement for the AhR domain in Pai-2 expression, we generated ANA-1 cells stably transfected with AhR Δ C (an activation domain-deficient mutant) and AhR Y9F (the mutant with attenuated DNA binding) (18). Compared with the expression in stable ANA-1 cells transfected with full-length AhR, neither of the cell lines transfected with AhR Δ C or AhR Y9F significantly expressed Pai-2 (Fig. 6B, bars 3 to 6, 9, and 10). These results indicate that both the activation and DNA binding domains of AhR were required for AhR-dependent Pai-2 expression. Co-IP analysis using these AhR mutants showed that the N-terminal region of AhR (AhR Δ C mutant) interacted with p65 (Fig. 6C).

DISCUSSION

AhR was originally found as a transcription factor that was involved in the induction of xenobiotic-metabolizing CYP1A1 by TCDD and other PAHs and has been found to act as a multifunctional regulatory factor in areas ranging from drug metabolism to innate immunity, providing protection against invading xenobiotics. Close investigation of the phenotypes of AhR KO mice revealed that they seem to suffer from morbidity from impaired immunity and easily succumb to bacterial infection. We examined the susceptibility of AhR KO mice to LPS-induced septic shock and found that they were hypersensitive to LPS treatment and had increased secretion of proinflammatory cytokines, such as IL-1 β , TNF- α , IL-18, and IFN- γ (Fig. 1A and B). It has been reported that in endotoxic shock, IL-1 β and TNF- α are rapidly released and trigger a secondary

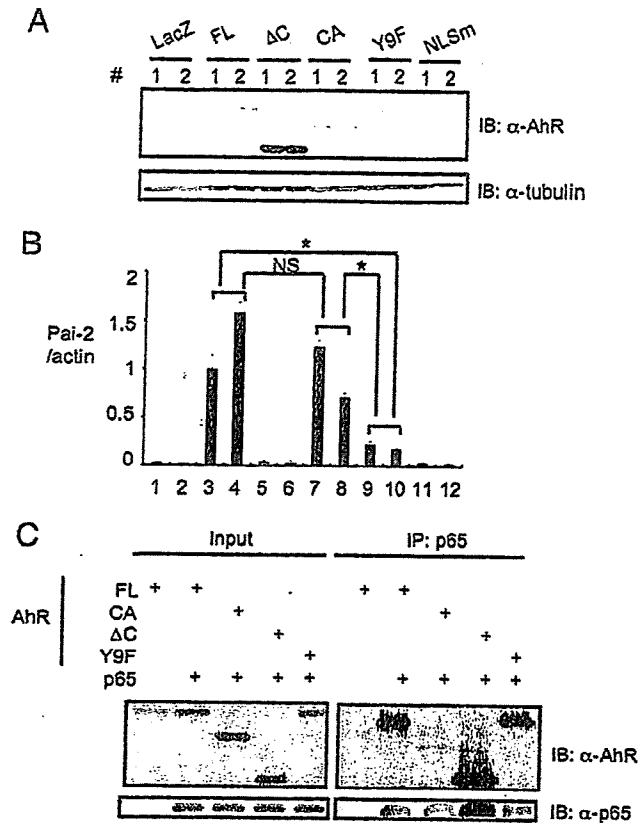


FIG. 6. Nuclear localization, activation, and DNA binding domains of AhR are required for AhR-dependent Pai-2 expression. **(A)** Immunoblot analysis of full-length AhR or mutants in LacZ or AhR transformant ANA-1 cells. Paired lanes labeled 1 and 2 show results from experiments using two independent transformants. **(B)** Relative expression levels of Pai-2 mRNA in ANA-1 cells transfected with LacZ or full-length AhR or mutants. Bars show quantification of the results in the 12 lanes in panel A; error bars show standard deviations. *, $P < 0.001$; NS, not significant. **(C)** Interaction of p65 and AhR mutants. Co-IP of p65 and full-length AhR or mutants expressed in 293T cells, using anti-p65 antibody. AhR FL (full-length) comprises amino acids 1 to 805, AhR ΔC comprises amino acids 1 to 544, and AhR CA comprises amino acids 1 to 276 and 419 to 805; in AhR Y9F, Y9 was mutated to F; and in AhR NLSm 37R, 38E, and 39R were mutated to A, G, and S, respectively. IB, immunoblot; α, anti; +, present.

inflammatory cascade that is dependent on the transcription factor NF- κ B (10). Mice with a macrophage-specific conditional deletion of AhR (AhR^{lox/-}::LysM Cre) were more susceptible to LPS-induced septic shock than AhR^{lox/-} mice, indicating that the dysfunction of macrophages due to AhR deficiency is one of the major causes of the enhanced susceptibility of AhR KO mice to LPS-induced septic shock (Fig. 2A). Consistent with these observations, isolated AhR KO BMDM secreted much larger amounts of IL-1 β and had a slight increase in TNF- α in response to LPS (Fig. 2B). Since IL-1 β mRNA levels were not altered between AhR KO and AhR WT BMDM (Fig. 2C), the increased IL-1 β secretion is probably not due to the enhanced synthesis but, rather, is likely due to enhanced processing of IL-1 β . (16).

We thought that this IL-1 β oversecretion by AhR-deficient macrophages might provide clues as to how AhR functions as

a physiological immunosuppressor. Microarray analyses to comprehensively investigate the AhR-dependent changes in gene expression that were responsible for increased IL-1 β secretion revealed that the levels of expression of Pai-2 and Bcl-2 mRNA were markedly reduced in AhR KO BMDM, which was confirmed by real-time PCR (Fig. 3B). Reconstitution experiments with adenoviruses showed that only Pai-2 expression could significantly suppress IL-1 β oversecretion in AhR KO macrophages, while no suppressive effect was observed with Bcl-2 expression (Fig. 3C). It has been reported that there are several pathways for processing IL-1 β that lead to its secretion (16). These results indicate that Pai-2 and Bcl-2 are differentially involved in these pathways. Recently, in experiments using Δ IKK β myeloid mice, Pai-2 has been reported to suppress IL-1 β secretion, acting downstream of NF- κ B (10). The IL-1 β processing that is regulated by the inflammasome involves caspase-1 (16). Consistent with these observations, treatment with caspase inhibitors, Z-YVAD-FMK and Z-VAD-FMK markedly reduced the secretion of IL-1 β in AhR KO BMDM (Fig. 3A). It has also been reported that IL-18 processing is regulated by the same mechanism as IL-1 β , which is consistent with the marked increase in plasma IL-18 levels ($P < 0.001$) observed in LPS-injected AhR KO mice (Fig. 1B). Stimulation of the inflammasome involving caspase-1 usually requires secondary signals, such as high ATP concentrations. Interestingly, however, the IL-1 β oversecretion resulting from AhR deficiency did not seem to require any other stimulation besides LPS, which is in accordance with the report on the IKK β Amyeloid mice (10). Further investigation will be required to address the molecular details of Pai-2-regulated IL-1 β secretion.

Although it has been reported that Pai-2 mRNA was induced by a typical AhR ligand, TCDD (27), we did not find any obvious XRE sequences (GCGTG) in the 5-kb regions upstream or downstream of the transcription start site of the mouse Pai-2 promoter. However, these promoter regions rendered a reporter gene responsive to LPS (Fig. 5A and E). This sequence search suggested that AhR might not regulate Pai-2 gene expression in the canonical way (i.e., heterodimerized with Arnt) and led us to investigate whether Arnt was involved in LPS-induced Pai-2 regulation. In experiments with Arnt-deficient and Arnt siRNA-expressing macrophages, we demonstrated that AhR enhanced Pai-2 expression in an Arnt-independent manner (Fig. 4D; also see Fig. S1 in the supplemental material). Arnt2 is considered to be another possible alternative (11), but we have previously shown that AhR interacts predominantly with Arnt but not with Arnt2 (27). Therefore, it is highly likely that AhR enhances Pai-2 expression independently of Arnt family proteins (11). It was previously reported that LPS induced Pai-2 expression through activation of NF- κ B (21) and that AhR physically interacted with p65 (31) to activate or inhibit gene expression in a context-dependent manner (31). In our reporter gene assay using RAW 264.7 cells, the Pai-2 reporter gene required both NF- κ B and AhR for a high level of expression in response to LPS treatment (Fig. 5A). In AhR KO macrophages, LPS treatment induced nuclear translocation of p65 (Fig. 5B), but it was not recruited to the NF- κ B-binding site of the Pai-2 gene, which confers LPS inducibility (Fig. 5E), suggesting that AhR is required for recruitment of p65 to this site, which may be a

crossing point between AhR and NF- κ B signaling pathways. In WT macrophages, AhR and p65 were recruited to the same DNA sequence by the LPS treatment (Fig. 5E), and they interacted directly (Fig. 5C and 6C), leading to the recruitment of PolIII to the TATA sequence of the transcription initiation site. In contrast, p65 was recruited to the Cox-2 promoter in response to LPS treatment in AhR KO macrophages. The detailed molecular basis for how p65 binds differentially to the Pai-2 and Cox-2 genes remains to be investigated.

It was also reported that AhR interacts with RelB on chemokine promoters, such as IL-8, in response to TCDD treatment, enhancing their expression (33). Although an AhR-RelB binding DNA sequence, designated RelBAhRE (GGGTGC AT), was found near the NF- κ B site in the Pai-2 promoter, the expression of the Pai-2 (-2.7 kb) Luc reporter gene was not enhanced by RelB and AhR coexpression (data not shown), suggesting that RelB may not function as a partner for AhR in inducing Pai-2 expression. Since the AhR DNA binding activity was suggested by the results of the experiment using the AhR Y9F mutant to be required for AhR-dependent Pai-2 expression (Fig. 6B, bars 3, 4, 9, and 10), the possibility could be raised that an AhR and p65 heterodimer might work as a transcription factor by binding the RelBAhRE sequence. However, the experiments using the reporter gene containing a tandem arrangement of four RelBAhRE sequences did not show enhanced expression of the reporter gene expression with coexpression of AhR and p65. It remains to be investigated in detail how AhR and p65 activate the Pai-2 promoter. AhR has been reported to have the nuclear localization signal and nuclear export signal sequences and to shuttle between nucleus and cytoplasm. Inhibition of nuclear export of AhR by trichomycin B or phosphorylation reportedly leads to the accumulation of AhR in the nucleus (12). Consistent with these findings, a small part of AhR was observed in the nuclei of macrophages under normal conditions. Upon treatment with LPS, nuclear AhR should accumulate due to phosphorylation downstream of the LPS signaling pathway or p65, reported to be translocated into the nucleus (21), should be recruited to the Pai-2 promoter with the nuclear AhR.

Recently, there have been growing lines of evidence that AhR plays a crucial role in differentiation of the Th cell subsets Th1, Treg, and Th17 from naive CD4 T cells. It was reported that differentiation of these regulatory T cells from AhR KO naive T cells was significantly impaired under their respective polarizing conditions. AhR is reported to be highly induced under these conditions (14, 20, 23, 32), and AhR ligands further stimulated the tendency to their respective differentiations by molecular mechanisms that are largely unknown. In macrophages, AhR was also induced by LPS treatment (Fig. 4A and B) and negatively regulated the secretion of certain inflammatory cytokines, such as IL-1 β and IL-18, most likely through the expression of Pai-2. Since AhR is a ligand-activated transcription factor and is known to be ubiquitously expressed in immune cells (13), this raises the possibility that an appropriate AhR ligand may be useful for treating patients with inflammatory disorders.

ACKNOWLEDGMENTS

We thank L. Varesio for kindly providing ANA-1 cells and Y. Watanabe and S. Ooba for mouse maintenance. We also thank Y. Nemoto for clerical work.

This work was funded in part by Solution Oriented Research for Science and Technology from Japan Science and Technology, Japan Science and Technology Agency, Kawaguchi, Japan, and by a grant for Scientific Research from the Ministry of Health, Labor and Welfare, Japan.

REFERENCES

- Abbott, B., J. Schmid, J. Pitt, A. Buckalew, C. Wood, G. Held, and J. Diliberto. 1999. Adverse reproductive outcomes in the transgenic Ah receptor-deficient mouse. *Toxicol. Appl. Pharmacol.* 155:62-70.
- Baba, T., J. Mimura, N. Nakamura, N. Harada, M. Yamamoto, K. Morohashi, and Y. Fujii-Kuriyama. 2005. Intrinsic function of the aryl hydrocarbon (dioxin) receptor as a key factor in female reproduction. *Mol. Cell. Biol.* 25:10040-10051.
- Blasi, E., D. Radzioch, S. Durum, and L. Varesio. 1987. A murine macrophage cell line, immortalized by v-raf and v-myc oncogenes, exhibits normal macrophage functions. *Bur. J. Immunol.* 17:1491-1498.
- Bradley, M., L. Zhou, and S. Smale. 2003. C/EBP β regulation in lipopolysaccharide-stimulated macrophages. *Mol. Cell. Biol.* 23:4841-4858.
- Bruet, J., N. Bruet-Sedano, F. Luciano, D. Zhai, R. Balpai, C. Xu, C. Kress, B. Bailly-Maitre, X. Li, A. Osterman, S. Matsuzawa, A. Tersikikh, B. Faustin, and J. Reed. 2007. Bcl-2 and Bcl-XL regulate proinflammatory caspase-1 activation by interaction with NALP1. *Cell* 129:45-56.
- Fernandez-Salguero, P., D. Hilbert, S. Rudikoff, J. Ward, and F. Gonzalez. 1996. Aryl-hydrocarbon receptor-deficient mice are resistant to 2,3,7,8-tetrachlorodibenzo-p-dioxin-induced toxicity. *Toxicol. Appl. Pharmacol.* 140:173-179.
- Fernandez-Salguero, P., T. Pineau, D. Hilbert, T. McPhail, S. Lee, S. Kimura, D. Nebert, S. Rudikoff, J. Ward, and F. Gonzalez. 1995. Immune system impairment and hepatic fibrosis in mice lacking the dioxin-binding Ah receptor. *Science* 268:722-726.
- Fernandez-Salguero, P., J. Ward, J. Sundberg, and F. Gonzalez. 1997. Lesions of aryl-hydrocarbon receptor-deficient mice. *Vet. Pathol.* 34:605-614.
- Fujii-Kuriyama, Y., and J. Mimura. 2005. Molecular mechanisms of AhR functions in the regulation of cytochrome P450 genes. *Biochem. Biophys. Res. Commun.* 338:311-317.
- Greten, F., M. Arkan, J. Bollrath, L. Hsu, J. Goode, C. Miethling, S. Gökten, M. Neuehahn, J. Hierer, S. Paxian, N. Van Rooijen, Y. Xu, T. O'Carin, B. Jaffee, D. Busch, J. Dyrster, R. Schmid, L. Eckmann, and M. Karin. 2007. NF- κ B is a negative regulator of IL-1 β secretion as revealed by genetic and pharmacological inhibition of IKK β . *Cell* 130:918-931.
- Hirose, K., M. Morita, M. Ema, J. Mimura, H. Hamada, H. Fujii, Y. Saijo, O. Gotoh, K. Sogawa, and Y. Fujii-Kuriyama. 1996. cDNA cloning and tissue-specific expression of a novel basic helix-loop-helix/PAS factor (Arnt2) with close sequence similarity to the aryl hydrocarbon receptor nuclear translocator (Arnt). *Mol. Cell. Biol.* 16:1706-1713.
- Ikata, T., Y. Kobayashi, and K. Kawajiri. 2004. Cell density regulates intracellular localization of aryl hydrocarbon receptor. *J. Biol. Chem.* 279:19209-19216.
- Kerkvliet, N. 2009. AHR-mediated immunomodulation: the role of altered gene transcription. *Biochem. Pharmacol.* 77:746-760.
- Kimura, A., T. Naka, K. Nohara, Y. Fujii-Kuriyama, and T. Kishimoto. 2008. Aryl hydrocarbon receptor regulates Stat1 activation and participates in the development of Th17 cells. *Proc. Natl. Acad. Sci. USA* 105:9721-9726.
- Lund, A., M. Guens, B. Nuñez, and M. Walker. 2006. Characterizing the role of endothelin-1 in the progression of cardiac hypertrophy in aryl hydrocarbon receptor (AhR) null mice. *Toxicol. Appl. Pharmacol.* 212:127-135.
- Martinon, F., and J. Tschopp. 2007. Inflammatory caspases and inflammasomes: master switches of inflammation. *Cell Death Differ.* 14:10-22.
- Mimura, J., K. Yamashita, K. Nakamura, M. Morita, T. Takagi, K. Nakao, M. Ema, K. Sogawa, M. Yasuda, M. Katsuki, and Y. Fujii-Kuriyama. 1997. Loss of teratogenic response to 2,3,7,8-tetrachlorodibenzo-p-dioxin (TCDD) in mice lacking the Ah (dioxin) receptor. *Genes Cells* 2:645-654.
- Minsavage, G. D., S. Park, and T. A. Gasiewicz. 2004. The aryl hydrocarbon receptor (AhR) tyrosine 9, a residue that is essential for AhR DNA binding activity, is not a phosphoresidue but augments AhR phosphorylation. *J. Biol. Chem.* 279:20582-20593.
- Muruve, D., V. Pétrilli, A. Zalus, L. White, S. Clark, P. Ross, R. Parks, and J. Tschopp. 2008. The inflammasome recognizes cytosolic microbial and host DNA and triggers an innate immune response. *Nature* 452:103-107.
- Negishi, T., Y. Kato, O. Ooneda, J. Mimura, T. Takada, H. Mochizuki, M. Yamamoto, Y. Fujii-Kuriyama, and S. Furusako. 2005. Effects of aryl hydrocarbon receptor signaling on the modulation of TH1/TH2 balance. *J. Immunol.* 175:7348-7356.
- Park, J., F. Greten, A. Wong, R. Westrick, J. Arthur, K. Otsu, A. Hoffmann, M. Montminy, and M. Karin. 2005. Signaling pathways and genes that inhibit pathogen-induced macrophage apoptosis—CREB and NF- κ B as key regulators. *Immunity* 23:319-329.
- Petrulis, J., and G. Perdew. 2002. The role of chaperone proteins in the aryl hydrocarbon receptor core complex. *Chem. Biol. Interact.* 141:25-40.

23. Quintana, F., A. Basso, A. Iglesias, T. Korn, M. Farez, E. Bettelli, M. Caccamo, M. Ouksa, and H. Weiner. 2008. Control of T(reg) and T(H)17 cell differentiation by the aryl hydrocarbon receptor. *Nature* 453:65-71.
24. Schmidt, J., G. Su, J. Reddy, M. Simon, and C. Bradfield. 1996. Characterization of a murine Ahr null allele: involvement of the Ah receptor in hepatic growth and development. *Proc. Natl. Acad. Sci. USA* 93:6731-6736.
25. Schreiber, E., P. Matthias, M. Müller, and W. Schaffner. 1989. Rapid detection of octamer binding proteins with 'mini-extracts,' prepared from a small number of cells. *Nucleic Acids Res.* 17:6419.
26. Schwartz, B., and J. Bradshaw. 1992. Regulation of plasminogen activator inhibitor mRNA levels in lipopolysaccharide-stimulated human monocytes. Correlation with production of the protein. *J. Biol. Chem.* 267:7089-7094.
27. Sekine, H., J. Mimura, M. Yamamoto, and Y. Fujii-Kuriyama. 2006. Unique and overlapping transcriptional roles of arylhydrocarbon receptor nuclear translocator (Arnt) and Arnt2 in xenobiotic and hypoxic responses. *J. Biol. Chem.* 281:37507-37516.
28. Sogawa, K., R. Nakano, A. Kobayashi, Y. Kikuchi, N. Ohe, N. Matsushita, and Y. Fujii-Kuriyama. 1995. Possible function of Ah receptor nuclear translocator (Arnt) homodimer in transcriptional regulation. *Proc. Natl. Acad. Sci. USA* 92:1936-1940.
29. Reference deleted.
30. Takagi, S., H. Tojo, S. Tomita, S. Sano, S. Itami, M. Hara, S. Inoue, K. Horie, G. Kondoh, K. Hosokawa, F. Gonzalez, and J. Takeda. 2003. Alteration of the 4-sphinganine scaffolds of ceramides in keratinocyte-specific Arnt-deficient mice affects skin barrier function. *J. Clin. Investig.* 112:1372-1382.
31. Tian, Y., S. Ke, M. Denison, A. Rabson, and M. Gallo. 1999. Ah receptor and NF-kappaB interactions, a potential mechanism for dioxin toxicity. *J. Biol. Chem.* 274:510-515.
32. Veldhoen, M., K. Hirota, A. Westendorf, J. Buer, L. Dumoutier, J. Renaud, and B. Stuckinger. 2008. The aryl hydrocarbon receptor links T(H)17-cell-mediated autoimmunity to environmental toxins. *Nature* 453:106-109.
33. Vogel, C., E. Sciallo, W. Li, P. Wong, G. Lazennec, and F. Matsumura. 2007. RelB, a new partner of aryl hydrocarbon receptor-mediated transcription. *Mol. Endocrinol.* 21:2941-2955.

Gene Expression Profiling and Cellular Distribution of Molecules with Altered Expression in the Hippocampal CA1 Region after Developmental Exposure to Anti-Thyroid Agents in Rats

Yukie SAEGUSA^{1,2}, Gye-Hyeong WOO³, Hitoshi FUJIMOTO³, Kaoru INOUE³, Miwa TAKAHASHI³, Masao HIROSE^{3,4}, Katsuhide IGARASHI⁵, Jun KANNO⁵, Kunitoshi MITSUMORI¹, Akiyoshi NISHIKAWA³ and Makoto SHIBUTANI¹*

¹Laboratory of Veterinary Pathology, Tokyo University of Agriculture and Technology, 3-5-8 Saiwai-cho, Fuchu-shi, Tokyo 183-8509, ²Pathogenetic Veterinary Science, United Graduate School of Veterinary Sciences, Gifu University, 1-1 Yanagido, Gifu-shi, Gifu 501-1193, ³Division of Pathology and ⁵Division of Molecular Toxicology, National Institute of Health Sciences, 1-18-1 Kamiyoga, Setagaya-ku, Tokyo 158-8501 and ⁴Food Safety Commission, Akasaka Park Bld. 22nd F., 5-2-20 Akasaka, Minato-ku, Tokyo 100-8989, Japan

(Received 6 September 2009/Accepted 8 October 2009/Published online in J-STAGE 27 November 2009)

ABSTRACT. To determine whether developmental hypothyroidism causes permanent disruption of neuronal development, we first performed a global gene expression profiling study targeting hippocampal CA1 neurons in male rats at the end of maternal exposure to anti-thyroid agents on weaning (postnatal day 20). As a result, genes associated with nervous system development, zinc ion binding, apoptosis and cell adhesion were commonly up- or down-regulated. Genes related to calcium ion binding were up-regulated and those for myelination were often down-regulated. We, then, examined immunohistochemical cellular distribution of Ephrin type A receptor 5 (EphA5) and Tachykinin receptor (Tacr)-3, those selected based on the gene expression profiles, in the hippocampal formation at the adult stage (11-week-old) as well as at the end of exposure. At weaning, both EphA5- and Tacr3-immunoreactive cells with strong intensities appeared in the pyramidal cell layer or stratum oriens of the hippocampal CA1 region. Although the magnitude of the change was decreased at the adult stage, Tacr3 in the CA1 region showed a sustained increase in expressing cells until the adult stage after developmental hypothyroidism. On the other hand, EphA5-expressing cells did not show sustained increase at the adult stage. The results suggest that developmental hypothyroidism caused sustained neuronal expression of Tacr3 in the hippocampal CA1 region, probably reflecting a neuroprotective mechanism for mismigration.

KEY WORDS: developmental hypothyroidism, EphA5, hippocampal CA1 region, Tacr3.

J. Vet. Med. Sci. 72(2): 187-195, 2010

Thyroid hormones are essential for normal fetal and neonatal brain development. They control neuronal and glial proliferation in definitive brain regions and regulate neural migration and differentiation [12, 18, 21]. In humans, maternal hypothyroxinemia, early in pregnancy, may have adverse effects on fetal brain development and importantly, even mild-moderate hypothyroxinemia may result in suboptimal neurodevelopment [4]. These results may increase the concern of thyroid hormone-disrupting chemicals in the environment.

Experimentally, developmental hypothyroidism leads to growth retardation, neurological defects and impaired performance on a variety of behavioral learning actions [1, 2]. Rat offspring exposed maternally to anti-thyroid agents such as 6-propyl-2-thiouracil (PTU) show brain retardation, with impaired neuronal migration and white matter hypoplasia involving limited axonal myelination and oligodendrocytic accumulation [6, 8, 21]. The outcome of this type of brain retardation is permanent and is accompanied by apparent structural and functional abnormalities. However, it is still unclear whether the molecular aberrations remain

in the retarded brain after maturation.

Histological lesion-specific gene expression profiling provides valuable information on the mechanisms underlying lesion development. We have established molecular analysis methods for DNA, RNA and proteins in paraffin-embedded small tissue specimens utilizing an organic solvent-based fixative, methacarn, with high performance close to that achieved with unfixed frozen tissue specimens [22, 26, 27]. We have previously applied these techniques to analyze global gene expression changes in microdissected lesions [23, 28].

Hippocampal CA1 region is a well-known target of developmental hypothyroidism [8], and we, in our recent study, detected a distribution variability of hippocampal CA1 pyramidal neurons reflecting mismigration in rat offspring at the adult stage after developmental exposure to anti-thyroid agents [24]. The present study was performed to determine whether developmental hypothyroidism triggers sustained aberrations in neuronal development associated with neuronal mismigration until the adult stage. For this purpose, we first performed a global gene expression profiling of the CA1-pyramidal cell layer in rat offspring at the end of developmental exposure to anti-thyroid agents. To distinguish chemical-specific expression changes from hypothyroidism-linked ones, two different anti-thyroid

* CORRESPONDENCE TO: SHIBUTANI, M., Laboratory of Veterinary Pathology, Tokyo University of Agriculture and Technology, 3-5-8 Saiwai-cho, Fuchu-shi, Tokyo 183-8509, Japan.
e-mail: mshibuta@cc.tuat.ac.jp

agents, PTU and 2-mercapto-1-methylimidazole (MMI), were used, and dose-related responses were also examined with PTU. To extract the neuronal cell layer-specific gene expression profile, microdissection technique was applied for microarray analysis. Based on the expression profiles obtained, cellular localization of the molecules showing altered expression were then immunohistochemically examined in the hippocampus at the adult stage as well as at the end of the developmental exposure.

MATERIALS AND METHODS

Chemicals and animals: 6-propyl-2-thiouracil (PTU; CAS No. 51-52-5) and methimazole (2-mercapto-1-methylimidazole: MMI; CAS No. 60-56-0) were obtained from Sigma Chemical Co. (St. Louis, MO, U.S.A.). Pregnant Crj:CD[®](SD)IGS rats were purchased from Charles River Japan Inc. (Yokohama, Japan) at gestation day (GD) 3 (appearance of vaginal plugs was designated as GD 0). Animals were housed individually in polycarbonate cages with wood chip bedding, maintained in an air-conditioned animal room (temperature: $24 \pm 1^\circ\text{C}$; relative humidity: $55 \pm 5\%$) with a 12-hr light/dark cycle and allowed *ad libitum* access to food and tap water. A soy-free diet (Oriental Yeast Co., Ltd., Tokyo, Japan) was chosen as the basal diet for the maternal animals to eliminate possible phytoestrogen effects [10], and water was given *ad libitum* throughout the experimental period including the 1-week acclimation period.

Animal experiments: The animal experiments were identical to those in a previous study [24]. In brief, maternal animals were randomly divided into four groups including untreated controls. Eight dams per group were treated with 3 or 12 ppm of PTU or 200 ppm of MMI in the drinking water from GD 10 to postnatal day (PND) 20 (PND 0: the day of delivery). On PND 2, the litters were culled randomly, leaving four male and four female offspring. On PND 20, 20 male and 20 female offspring (at least one male and one female per dam) per group were subjected to prepubertal necropsy [13, 24].

The remaining animals were maintained until postnatal week (PNW) 11. All offspring consumed the CRF-1 basal diet and tap water *ad libitum* from PND 21 onwards. At PNW 11, all pups were subjected to adult stage necropsy [13, 24].

All animals used in the present study were weighed and sacrificed by exsanguination from the abdominal aorta under deep anesthesia. These protocols were reviewed in terms of animal welfare and approved by the Animal Care and Use Committee of the National Institute of Health Sciences, Japan.

Preparation of tissue specimens and microdissection: For microarray and subsequent real-time RT-PCR analyses, the whole brain of male offspring was removed at prepubertal necropsy on PND 20 ($n=4/\text{group}$) and was fixed with methacarn solution for 2 hr at 4°C [22]. Coronal brain slices taken at the position of -3.5 mm from the bregma were

dehydrated and embedded in paraffin. The embedded tissue blocks were stored at 4°C until tissue sectioning for microdissection [9].

For microdissection, $4\text{-}\mu\text{m}$ -thick sections between ten $20\text{-}\mu\text{m}$ -thick serial sections were prepared. The $4\text{-}\mu\text{m}$ -thick sections were stained with hematoxylin and eosin for confirmation of anatomical orientation of the hippocampal substructure to aid microdissection. The $20\text{-}\mu\text{m}$ -thick sections were mounted onto PEN-foil film (Leica Microsystems GmbH, Welzlar, Germany) overlaid on glass slides, dried in an incubator overnight at 37°C , and then stained using an LCM staining kit (Ambion, Inc., Austin, TX, U.S.A.). Bilateral sides of the hippocampal CA1 pyramidal cell layer in the sections were subjected to laser microbeam microdissection (Leica Microsystems GmbH) (Fig. 1). Twenty sections from each animal were used for microdissection, and the bilateral microdissected samples were collected and stored in separate 1.5-ml sample tubes at -80°C until the extraction of total RNA.

RNA preparation, amplification and microarray analysis: Total RNA extraction from hippocampal CA1 samples, quantitation of the RNA yield, and amplification of RNA samples were performed using previously described methods [9, 28].

For microarray analysis, second-round-amplified biotin-labeled antisense RNAs were subjected to hybridization with a GeneChip[®] Rat Genome 230 2.0 Array (Affymetrix, Inc., Santa Clara, CA, U.S.A.), as previously described [28].

The selection of genes and normalization of the expression data were performed using GeneSpring[®] software (ver7.2, Silicon Genetics, Redwood City, CA, U.S.A.). Per chip normalization was performed according to a previously described method [28]. Genes showing signals judged to be "absent" in all eight samples of untreated controls and in the anti-thyroid agent-exposed group were excluded. Genes

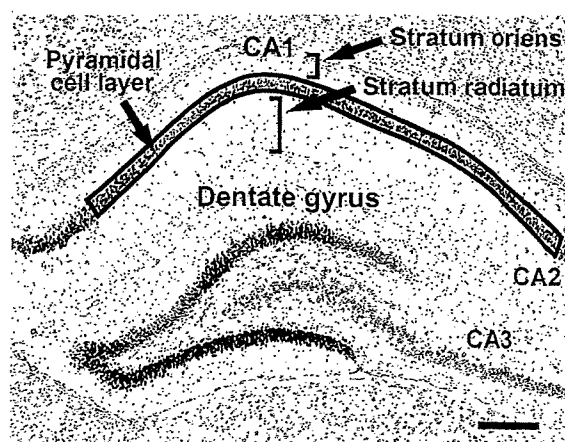


Fig. 1. Overview of the hippocampal formation of a male rat at postnatal day 20 stained with hematoxylin and eosin. Bar= $200\text{ }\mu\text{m}$. The CA1 pyramidal cell layer, enclosed by a solid line, was microdissected for the microarray and subsequent real-time RT-PCR analyses. The number of cells immunoreactive for the candidate molecules in this area was normalized for the length of CA1 used.

showing expression changes with differences of at least twofold in magnitude from the untreated controls were selected, and the "presence" signal in more than 3/4 of samples in each group showing higher expression values were selected. Genes showing altered expression in common in the anti-thyroid agent-exposed groups were also selected.

Real-time RT-PCR: Quantitative real-time RT-PCR was performed to confirm the expression values obtained with microarrays using an ABI Prism 7000 Sequence Detection System (Applied Biosystems Japan, Tokyo, Japan). Genes those showing altered expression (≥ 2 -fold, ≤ 0.5 -fold) in common in the anti-thyroid agent-exposed groups as compared with untreated control offspring were randomly selected, irrespective of the presence or absence of statistically significant difference. As a result, the following seven genes (four up-regulated and three down-regulated) with known function were selected as targets: Tachykinin receptor 3 (*Tacr3*), Calbindin 1, Slit homolog 2 (*Drosophila*) and Pleomorphic adenoma gene-like 1 (*Plagl1*) as up-regulated examples, and Myelin-associated oligodendrocytic basic protein (*Mobp*), Endothelial differentiation, sphingolipid G-protein-coupled receptor, 8 and CCAAT/enhancer binding protein as down-regulated. RT was performed using first-round antisense RNAs prepared for microarray analysis. For real-time PCR analysis of the genes selected, ABI Assays-on-Demand™ TaqMan® probe and primer sets from Applied Biosystems (available at <https://products.appliedbiosystems.com/ab/en/US/adirect/ab?cmd=catNavigate2&catID=601267>)($n=4$ /group) were used. For quantification of the expression data, a standard curve method was applied. The expression values were normalized to two housekeeping genes, Glyceraldehyde 3-phosphate dehydrogenase and Hypoxanthine-guanine phosphoribosyltransferase.

Immunohistochemistry: To evaluate the immunohistochemical distribution of the molecules selected by microarray analysis, the brains of male pups obtained at PND 20 or PNW 11 were fixed in Bouin's solution at room temperature overnight. Six animals were used as untreated controls, six for 200 ppm MMI, eight for 3 ppm PTU, and nine for 12 ppm PTU on PND 20. On PNW 11, 10 animals were used as untreated controls and 10 for 200 ppm MMI, nine for 3 ppm PTU, and six for 12 ppm PTU.

Immunohistochemistry was performed on the brain tissue sections of PND 20 and PNW 11 animals with antibodies against Ephrin type A receptor 5 (EphA5; rabbit IgG, 1:50; Abcam, Cambridge, U.K.) and Tacr3 (rabbit polyclonal antibody, 1:3,000, Novus Biologicals, Inc., Littleton, CO, U.S.A.), which were incubated with the tissue sections overnight at 4°C. Antigen retrieval treatment was not performed for these antigens. Immunodetection was carried out using a VECTASTAIN® Elite ABC kit (Vector Laboratories Inc., Burlingame, CA, U.S.A.) with 3,3'-diaminobenzidine/H₂O₂ as the chromogen, as previously described [23]. The sections were then counterstained with hematoxylin and cover-slipped for microscopic examination.

With regard to EphA5, *Efna5*, a gene encoding the representative ligand for this receptor molecule [5], was found to

be up-regulated (≥ 2 -fold) by microarray analysis in all of the groups exposed to anti-thyroid agents in the present study (Table 1). Because distribution of EphA5 has been confirmed in the pyramidal cells of the hippocampal CA1 region at both developmental and adult stages in mice and at adult stage in humans [3, 17], we selected this molecule to examine distribution changes in the present study. Tacr3 was also up-regulated in all of the MMI and PTU groups by microarray analysis and real-time RT-PCR in the present study (Table 1). Expression of Tacr3 in the hippocampal CA1 pyramidal neurons has also been confirmed in rats [11], and therefore, we also selected this molecule for examination in the expression changes in the present study.

Morphometry of immunolocalized cells and apoptotic cells: EphA5- or Tacr3-immunoreactive cells distributed in the pyramidal cell layer or stratum oriens of the hippocampal CA1 region were bilaterally counted and normalized to the number in the length of the CA1 region measured (Fig. 1). Tacr3-immunoreactive cells in the subgranular zone of the dentate gyrus were also bilaterally counted and normalized for the number in the length of the granular zone measured. For quantitative measurement of each immunoreactive cellular component, digital photomicrographs at 100-fold magnification were taken using a BX51 microscope (Olympus Optical Co., Ltd., Tokyo, Japan) attached to a DP70 Digital Camera System (Olympus Optical Co., Ltd.), and quantitative measurements were performed using the WinROOF image analysis software package (version 5.7, Mitani Corp., Fukui, Japan).

Statistical analysis: Numerical data of the number of immunoreactive cells were assessed using Student's *t*-test to compare the untreated controls with each of the anti-thyroid agent-exposed groups when the variance was homogenous among the groups using a test for equal variance. If a significant difference in variance was observed, Aspin-Welch's *t*-test was used instead. The data for gene expression levels from real-time RT-PCR analysis were analyzed by the Kruskal-Wallis test, followed by Bartlett's test. When statistically significant differences were indicated, Dunnett's multiple test was used for comparisons with the untreated controls. For the microarray data, statistical analysis was performed with GeneSpring® software, and the significance of gene expression changes was analyzed by Student's *t*-test or ANOVA between the untreated controls and each of the anti-thyroid agent-exposed groups.

RESULTS

Microarray analysis: Figure 2 shows the Venn diagram of genes showing altered expression in the microdissected CA1 pyramidal neurons in the exposure groups in combination or individually in each exposure group. Many genes were found to be up- or down-regulated in common in two of the three groups. The numbers of genes classified into common categories between the groups or individually in each group were similar in terms of up- and down-regulated genes. The number of genes showing up- or down-regula-

Table 1. List of representative genes showing up- or down-regulation common to 2-mercapto-1-methylimidazole (MMI), 3 and 12 ppm 6-propyl-2-thiouracil (PTU) (≥ 2 -fold, ≤ 0.5 -fold)

Gene function	Accession No.	Gene title	Symbol	MMI	3 ppm PTU	12 ppm PTU
<i>Up-regulated genes (of 119 genes in total)</i>						
Nervous system development	AI101660	Slit homolog 2 (Drosophila)	Slit2	3.04	2.62	7.08
Nervous system development	NM_024358.1	Notch gene homolog 2 (Drosophila)	Notch2	2.52	2.01	2.02
Nervous system development	AW527295	Ephrin A5	EfnA5	3.12	3.46	4.31
Nervous system development	NM_053465.1	Fucosyltransferase 9	Fut9	2.13	6.75	2.11
Nervous system development	BE106256	Sparc/osteonectin, cwcv and kazal-like domains proteoglycan 1	Spock1	3.22	3.13	2.15
Calcium ion binding	X04280.1	Calbindin 1	Calb1	4.48	4.85	9.00
Calcium ion binding	BM386119	UDP-N-acetyl-alpha-D-galactosamine:polypeptide N-acetylgalactosaminyltransferase 3 (GalNAc-T3)	Galnt3	2.43	2.30	2.63
Calcium ion binding	BI279663	Desmocollin 2	Dsc2	2.82	2.04	5.62
Calcium ion binding	AI105369	Calmodulin-like 4	Calml4	3.40	2.25	5.59
Zinc ion binding	BE098686	Similar to Tnf receptor-associated factor 1	LOC687813	3.10	2.04	2.78
Zinc ion binding	BF562032	RAN binding protein 2	Ranbp2	3.49	2.67	2.78
Zinc ion binding	BF397925	ADAMTS-like 1	Adamts1	6.22	2.55	7.63
Zinc ion binding	BF395606	Splicing factor, arginine/serine-rich 7	Sf3f7	4.93	2.06	2.90
Apoptosis	NM_012760.1	Pleomorphic adenoma gene-like 1	Plagl1	3.10	4.28	6.86
Apoptosis	NM_057130.1	Harakiri, BCL2 interacting protein (contains only BH3 domain)	Hrk	2.63	2.73	3.18
Cell Adhesion	AA850909	Poliiovirus receptor-related 2	Pvr12	4.74	2.46	2.61
Cell Adhesion	AA819731	Hyaluronan and proteoglycan link protein 4	Hapln4	4.13	6.67	3.46
Cell Adhesion	BI287851	Collagen, type VI, alpha 2	Coll6a2	3.45	2.19	5.12
Ion channel activity	AA851939	FXYD domain-containing ion transport regulator 6	Fxyd6	4.73	2.61	7.85
Other	NM_017053.1	Tachykinin receptor 3	Tacr3	7.32	6.19	12.49
<i>Down-regulated genes (of 97 genes in total)</i>						
Nervous system development	NM_031018.1	Activating transcription factor 2	Atf2	0.41	0.36	0.36
Neuron migration	BF390065	Roundabout homolog 3 (Drosophila)	Robo3	0.06	0.31	0.04
Neuron differentiation	AF115249.1	Endothelial differentiation, sphingolipid G-protein-coupled receptor, 8	Edg8	0.40	0.06	0.08
Neuron differentiation	NM_024125.1	CCAAT/enhancer binding protein (C/EBP), beta	Cebpb	0.31	0.43	0.26
Myelination	X89638.1	Myelin-associated oligodendrocytic basic protein	Mobp	0.35	0.18	0.12
Myelination	NM_017190.1	Myelin-associated glycoprotein	Mag	0.47	0.36	0.29
Myelination	NM_022668.1	Myelin oligodendrocyte glycoprotein	Mog	0.44	0.32	0.19
Myelination	NM_012798.1	Mal, T-cell differentiation protein	Mal	0.37	0.28	0.28
Myelination	AA945178	Signal recognition particle receptor, B subunit transferrin	Srprb Tf	0.33	0.27	0.15
Zinc ion binding	NM_012566.1	Growth factor independent 1 transcription repressor	Gfi1	0.20	0.44	0.41
Zinc ion binding	AW529624	Zinc finger protein 91	Zfp91	0.33	0.32	0.38
Actin binding	AW522439	Ermin, ERM-like protein	Ermin	0.43	0.42	0.28
Apoptosis	BG377720	Solute carrier family 5 (sodium/glucose cotransporter), member 11	Slc5a11	0.25	0.19	0.19
Apoptosis	U21955.1	Eph receptor A	Epha7	0.34	0.48	0.18
Cell Adhesion	BM391100	Mucin 4, cell surface associated	Muc4	0.43	0.36	0.27
Other	AW435010	Protein tyrosine phosphatase, non-receptor type 3	Ptpn3	0.38	0.46	0.36
Other	AF312319.1	gamma-aminobutyric acid (GABA) B receptor 1	Gabbr1	0.33	0.41	0.39
Other	NM_053936.1	Endothelial differentiation, lysophosphatidic acid G-protein-coupled receptor, 2	Edg2	0.47	0.31	0.31

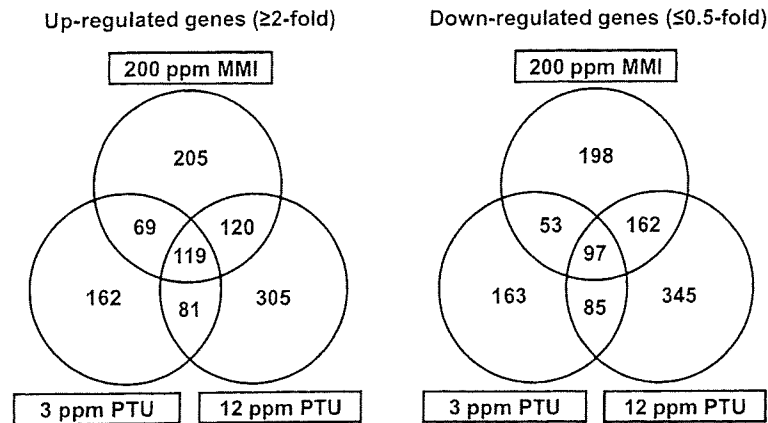


Fig. 2. Venn diagram of gene populations showing altered expression in the hippocampal CA1 pyramidal cell layer at postnatal day 20 in response to maternal exposure to propylthiouracil and/or 2-mercapto-1-methylimidazole compared with the untreated controls. (Left) Up-regulated genes (≥ 2 -fold). (Right) Down-regulated genes (≤ 0.5 -fold). Abbreviations: MMI, 2-mercapto-1-methylimidazole; PTU, 6-propyl-2-thiouracil.

Table 2. Validation of microarray data by real-time RT-PCR

Gene	200 ppm MMI			3 ppm PTU			12 ppm PTU		
	Microarray	Real-time RT-PCR normalized to		Microarray	Real-time RT-PCR normalized to		Microarray	Real-time RT-PCR normalized to	
		Hprt ^{a)}	Gapdh ^{b)}		Hprt	Gapdh		Hprt	Gapdh
Tacr3 ^{c)}	7.32 ± 2.21**	4.29 ± 1.27	4.08 ± 1.15*	6.19 ± 2.19**	3.46 ± 1.42	3.76 ± 1.51*	12.49 ± 1.56**	9.23 ± 3.00**	8.81 ± 1.60**
Calb1 ^{d)}	4.48 ± 0.66*	3.96 ± 0.74	3.67 ± 0.16	4.85 ± 2.53*	4.74 ± 2.48	4.93 ± 3.79	9.00 ± 1.85**	11.13 ± 2.13**	10.53 ± 3.26**
Slit2 ^{e)}	3.04 ± 0.79	2.83 ± 0.90	4.08 ± 1.15*	2.62 ± 1.16	1.33 ± 0.67	3.67 ± 1.51*	7.08 ± 2.15**	4.72 ± 2.57**	8.81 ± 1.60**
Plg11 ^{f)}	3.10 ± 1.57	12.67 ± 5.00	11.5 ± 7.50	4.28 ± 2.88	18.33 ± 6.00	19.00 ± 9.00*	6.86 ± 2.85**	30.67 ± 5.33**	27.00 ± 8.00**
Mobp ^{g)}	0.35 ± 0.15**	0.6 ± 0.22*	0.52 ± 0.16**	0.18 ± 0.07**	0.24 ± 0.07**	0.24 ± 0.05**	0.12 ± 0.02**	0.18 ± 0.04**	0.16 ± 0.04**
Edg8 ^{h)}	0.40 ± 0.11*	0.49 ± 0.16*	0.43 ± 0.13*	0.06 ± 0.05**	0.29 ± 0.10**	0.28 ± 0.08**	0.08 ± 0.07**	0.21 ± 0.07**	0.18 ± 0.03**
Cebpb ⁱ⁾	0.31 ± 0.06**	0.43 ± 0.04**	0.38 ± 0.06**	0.43 ± 0.18**	0.77 ± 0.07	0.76 ± 0.10	0.26 ± 0.04**	0.39 ± 0.16**	0.35 ± 0.22**

a) Hprt, Hypoxanthine-guanine phosphoribosyltransferase; b) Gapdh, Glyceraldehyde 3-phosphate dehydrogenase; c) Tacr3, Tachykinin receptor 3; d) Calb1, Calbindin 1; e) Slit2, Slit homolog 2 (*Drosophila*); f) Plg11, Pleomorphic adenoma gene-like 1; g) Mobp, Myelin-associated oligodendrocytic basic protein; h) Edg8, Endothelial differentiation, sphingolipid G-protein-coupled receptor, 8; i) Cebpb, CCAAT/enhancer binding protein (C/EBP), beta.

Values are mean ± SD (n=4) relative to the expression level in the untreated controls. Real-time RT-PCR analysis of Hprt and Gapdh was performed in the analysis of each target gene.

*, **: Significantly different from the untreated controls at $P < 0.05$ and $P < 0.01$, respectively (Dunnett's multiple comparison test).

tion in response to 12 ppm PTU was approximately 2-fold higher than that with 3 ppm PTU. The number of genes showing up- or down-regulation in response to 200 ppm MMI was in between that elicited by 3 or 12 ppm PTU. One-hundred nineteen genes were up-regulated in common by MMI and PTU, with PTU showing up-regulation from 3 ppm. On the other hand, 97 genes showed down-regulation in all MMI and PTU groups. Representative genes showing up- or down-regulation in all three groups are shown in the Table 1. Among the genes listed, genes associated with nervous system development, zinc ion binding, apoptosis and cell adhesion were commonly up- or down-regulated. Genes related to calcium ion binding were found to be up-regulated and those for myelination were often down-regulated.

Real-time RT-PCR analysis: For confirmation of the microarray data, four genes that were up-regulated and three that were down-regulated in response to anti-thyroid agents were selected for mRNA expression analysis by real-time RT-PCR and the results are summarized in Table 2.

In all exposure groups, many of the expression changes were similar in the two analysis systems, except for much higher expression of *Plg11* in all exposure groups by real-time RT-PCR as compared with findings from the microarray system.

Although we performed expression analysis of *EfnA5* by real-time RT-PCR, expression values were rather low with great variability between samples, and therefore, reliable quantitative data could not be obtained (data not shown).

Immunolocalization of EphA5 and Tacr3 in the hippoc-

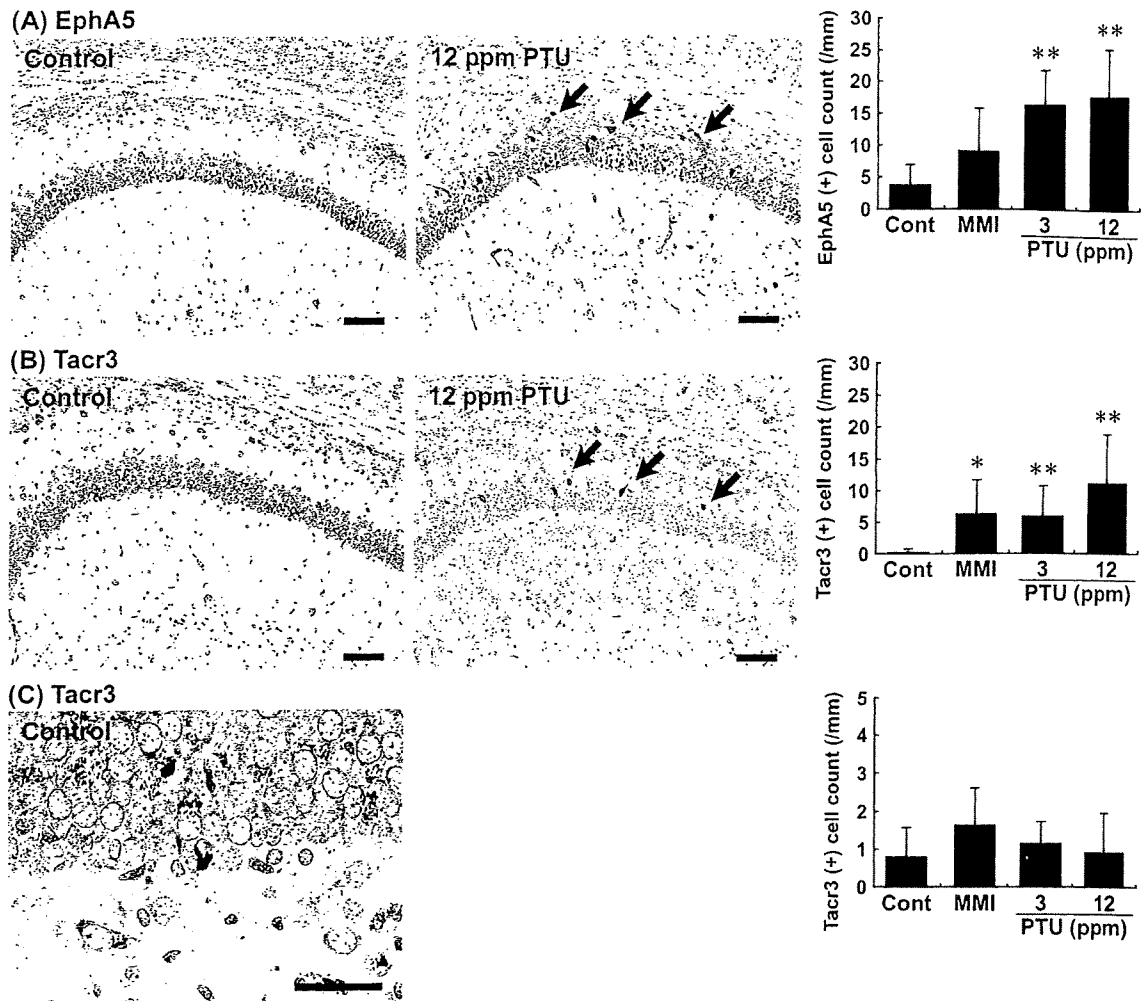


Fig. 3. Distribution of immunoreactive cells for EphA5 and Tacr3 in the hippocampal formation in rats at PND 20 after maternal exposure to anti-thyroid agents. (A) EphA5-immunoreactive cells with strong intensity located within the pyramidal cell layer and stratum oriens of the hippocampal CA1 region (arrows). Note the higher number of EphA5-positive cells in a case exposed to 12 ppm PTU (Right) as compared with the control animal (Left). Bar = 100 μ m. The graph shows the number of EphA5-positive cells/unit length (mm) of the CA1 region of the bilateral hemispheres. ** $P < 0.01$ versus untreated controls (Student's *t*-test). (B) Tacr3-immunoreactive cells with strong intensity located within the pyramidal cell layer and stratum oriens of the hippocampal CA1 region (arrows). Note the higher number of Tacr3-positive cells in a case exposed to 12 ppm PTU (Right) as compared with the control animal (Left). Bar = 100 μ m. The graph shows the number of Tacr3-positive cells/unit length (mm) of the CA1 region of bilateral hemispheres. * $P < 0.05$, ** $P < 0.01$ versus untreated controls (Student's *t*-test). (C) Tacr3-immunoreactive cells located in the subgranular zone of the dentate gyrus. Bar = 50 μ m. The graph shows the number of Tacr3-positive cells/unit length (mm) of the subgranular zone of bilateral hemispheres. Abbreviations: EphA5, Ephrin type A receptor 5; MMI, 2-mercapto-1-methylimidazole; PTU, 6-propyl-2-thiouracil; Tacr3, Tachykinin receptor 3.

ampal formation: Immunohistochemical localization of EphA5 and Tacr3 in the hippocampal formation was examined at PND 20 and PNW 11.

On PND 20, EphA5 showed weak immunoreactivity in the pyramidal neurons throughout the hippocampal formation in the untreated controls. This immunoreactivity was unchanged by exposure to anti-thyroid agents. On the other hand, very sparse distribution of strongly immunoreactive cells for EphA5 was observed in the region of the CA1 pyramidal cell layer and stratum oriens in the untreated control

animals, but immunoreactive cells were significantly increased showing scattered distribution by PTU at both 3 and 12 ppm (Fig. 3A). MMI-exposed animals also showed a small increase in the number of strongly positive cells with EphA5. Increased intensity in immunoreactivity of EphA5 was also observed in the gray matter consisting of neuropil at the stratum oriens of the CA1 region (Fig. 3A), and also in the molecular layer of the dentate gyrus at PND 20 after exposure to anti-thyroid agents, especially in PTU-exposed groups (data not shown).

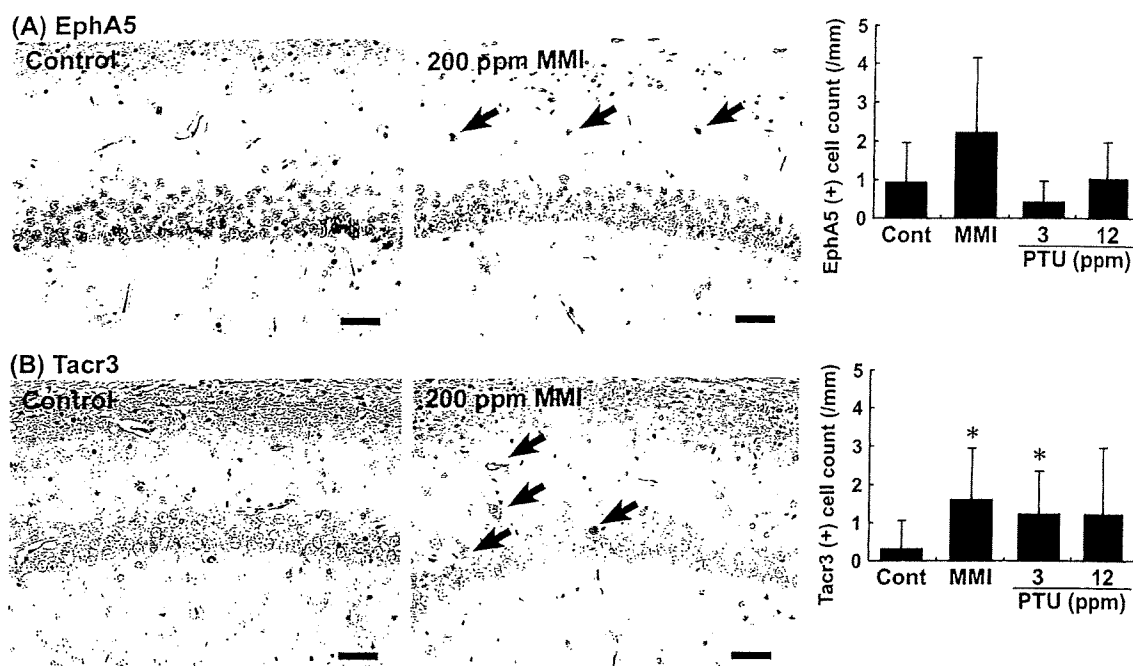


Fig. 4. Distribution of immunoreactive cells for EphA5 and Tacr3 in the hippocampal formation at PNW 11 of rats exposed maternally to anti-thyroid agents. (A) EphA5-immunoreactive cells with moderate staining intensity located within the pyramidal cell layer and stratum oriens of the hippocampal CA1 region. EphA5-positive cells in a case exposed to 200 ppm MMI (Right) as compared with the control animal (Left). The arrows show positive cells. Bar = 50 μ m. The graph shows the number of EphA5-positive cells/unit length (mm) of the CA1 region of the bilateral hemispheres. (B) Tacr3-immunoreactive cells with weak to moderate staining intensity located within the pyramidal cell layer and stratum oriens of the hippocampal CA1 region (arrows). Immunoreactivity is rather faint as compared with that observed at PND 20. Note the higher number of Tacr3-positive cells in a case exposed to 200 ppm MMI (Right) as compared with the control animal (Left). Bar = 50 μ m. The graph shows the number of Tacr3-positive cells/unit length (mm) of the CA1 region of bilateral hemispheres. * $P < 0.05$ versus untreated controls (Student's *t*-test). Abbreviations: EphA5, Ephrin type A receptor 5; MMI, 2-mercapto-1-methylimidazole; PTU, 6-propyl-2-thiouracil; Tacr3, Tachykinin receptor 3.

With regards to Tacr3, the number of positive cells was increased with a scattered distribution showing strong intensity in the CA1 region similarly to that of EphA5 in the animals exposed to MMI or PTU on PND 20, but they were mostly absent in the untreated controls (Fig. 3B). Similarly, Tacr3-immunoreactive cells were sparse in the subgranular zone of the dentate gyrus in the MMI and PTU-exposed animals and in the untreated controls, but there were no differences in the number of positive cells as compared with the untreated controls (Fig. 3C). In addition, increased intensity in neuropil-immunoreactivity of Tacr3 was also observed in the strata oriens and radiatum of the CA1 region in all exposure groups of anti-thyroid agents (Fig. 3B).

On PNW 11, EphA5 showed weak immunoreactivity in the pyramidal neurons throughout the hippocampal formation in the untreated controls. This immunoreactivity was unchanged by exposure to anti-thyroid agents. EphA5-immunoreactive cells with moderate staining intensity were very sparsely observed in the region of the CA1 pyramidal cell layer and stratum oriens in the untreated control animals. There was no statistically significant increase in the

number of these immunoreactive cells after exposure to PTU, while animals exposed to MMI showed a tendency for an increased number of immunoreactive cells (Fig. 4A). Increased neuropil-immunoreactivity of EphA5 as observed at PND 20 in exposure groups of anti-thyroid agents was mostly disappeared at PNW 11 (data not shown).

As well as at PND 20, Tacr3-immunoreactive cells were mostly absent in the untreated controls at PNW 11; however, a few immunoreactive cells with weak to moderate intensity were observed in the stratum oriens of the CA1 region in the animals exposed to anti-thyroid agents. There was a statistically significant difference in the animals treated with MMI or 3 ppm PTU compared with the untreated controls (Fig. 4B). Although the change was non-significant and lacked dose-dependence, 12 ppm PTU also showed an increasing tendency in the number of Tacr3-immunoreactive cells. In addition, increased neuropil-immunoreactivity of Tacr3 as observed at PND 20 in exposure groups of anti-thyroid agents was mostly disappeared at PNW 11 (data not shown).

DISCUSSION

In our recent study using rats [24], after maternal exposure to MMI or PTU, we detected typical hypothyroidism-related changes in the thyroid-related hormone levels, and hippocampal CA1 pyramidal neurons due to neuronal mis-migration, as previously reported [8]. We also observed white matter changes, which seem to be due to impaired oligodendroglial development [6, 21]. To visualize molecules related to impaired neuronal development, microdissected CA1 region-specific global gene expression profiling was performed in the present study using the same animals that were used in our previous study. Two recently published studies have used microarrays to examine the expression profiles in the cerebral cortex and hippocampus of genes linked to developmental hypothyroidism caused by maternal PTU-exposure [7, 19]. In accordance with these studies, the genes that were significantly down-regulated in the present study included those that play roles in myelination, such as *Mobp* and myelin-associated glycoprotein, suggestive of the reflection of suppressed myelination by developmental hypothyroidism [21]. However, the genes that were found to be up-regulated on microdissected CA1 pyramidal cell layer, including *Efna5* and *Tacr3*, in the present study, have not been identified in previous studies. This difference may be related to the target tissues collected and the methods used, including microdissection of CA1 pyramidal cell layer from paraffin-embedded sections in the present study versus manual dissection of the cortical tissues from unfixed tissues in the previous studies.

EphA5 is a tyrosine kinase receptor that is almost exclusively expressed in the nervous system [15]. EphA5 and its ligand are important in mediating axon guidance, topographic projection, development, cell migration and the plasticity of limbic structures [15]. In addition, the transient expression of EphA5 during development is correlated with early neurogenesis and the migration of differentiated cells in the midbrain [3]. Thus, although expression of EphA5 was mostly weak in the euthyroid CA1 pyramidal neurons at PND 20, the increased number of EphA5-expressing cells with strong intensity in the CA1 region during developmental hypothyroidism in the present study reflects the neuronal mis-migration caused by anti-thyroid agents. However, this increase was recovered after cessation of developmental hypothyroidism. Ephrins and their receptors are recently identified molecules and functional relationship between subfamily proteins is largely unknown; however, we, in the present study, found down-regulation of EphA7, another subfamily ephrin receptor, in all exposure groups of anti-thyroid agents (Table 1).

Tacr3, a member of the mammalian tachykinin peptide neurotransmitter/neuromodulator receptor family, is predominantly expressed in neurons in both the peripheral and central nervous systems, including the hippocampus [25]. There is increasing evidence of the role of Tacr3 on the survival and function of dopaminergic neurons. The survival of mesencephalic dopaminergic neurons during develop-

ment largely depends on excitatory inputs, and tachykinins, through their receptors, are reported to play role in excitation [20]. On the other hand, senktide, a Tacr3 agonist, activates dopaminergic neurons to stimulate the release of dopamine and serotonin, and hyperlocomotion in gerbils [14]. Abnormal excitatory action of D₂-like receptor, one of the major subtypes of dopaminergic receptors, was observed on glutamatergic transmission in the CA1 synapses in the adult stage of rats after developmental hypothyroidism, suggesting a permanent disruption of synaptic integration in the CA1 neural networks [16]. While the role of Tacr3 in the hippocampal CA1 region during development is not clear, the increase in Tacr3-positive cells with strong intensity in this region during developmental hypothyroidism suggests a cell survival effect of tachykinin-3. Although the magnitude of the change was decreased, as compared with that at the end of the developmental hypothyroidism, the increased number of Tacr3-positive cells in the CA1 region of MMI and 3 ppm PTU-exposed animals may be an outcome of permanent disruption of synaptic integration, as described by Oh-Nishi *et al.* [16]. However, sparse distribution of Tacr3-positive cells may reflect that impairment sustained in a small population of aberrantly migrated neurons.

In conclusion, in this study, we have shown gene expression profiles showing altered expression in response to developmental hypothyroidism by analysis on microdissected hippocampal CA1 pyramidal cell layer in rats. Immunohistochemical analysis of the two candidate molecules revealed that developmental hypothyroidism until weaning is associated with the persistence of Tacr3-expressing neurons until the adult stage in the CA1 region, suggestive of the reflection of permanent disruption of synaptic integration. These findings probably reflect a mechanism to facilitate cell survival of aberrantly developed neurons due to mis-migration.

ACKNOWLEDGMENT(S). We thank Miss Tomomi Morikawa for her technical assistance in conducting the animal study. We also thank Mrs. Shigeiko Suzuki and Miss Ayako Kaneko for their technical assistance in preparing the histological specimens. This work was supported in part by Health and Labour Sciences Research Grants (Research on Risk of Chemical Substances) from the Ministry of Health, Labour and Welfare of Japan. All of the authors disclose that there are no conflicts of interest that could inappropriately influence the outcomes of the present study.

REFERENCES

1. Akaike, M., Kato, N., Ohno, H. and Kobayashi, T. 1991. Hyperactivity and spatial maze learning impairment of adult rats with temporary neonatal hypothyroidism. *Neurotoxicol. Teratol.* 13: 317-322.
2. Comer, C. P. and Norton, S. 1982. Effects of perinatal methimazole exposure on a developmental test battery for neurobehavioral toxicity in rats. *Toxicol. Appl. Pharmacol.* 63: 133-141.
3. Cooper, M. A., Crockett, D. P., Nowakowski, R. S., Gale, N. W. and Zhou, R. 2009. Distribution of EphA5 receptor protein